

A New Virtual Reconstruction of the Ndotu Cranium

Gustavo Montiel ^{1,*}  and Carlos Lorenzo ^{1,2} ¹ Campus Catalunya, Universitat Rovira i Virgili, Av. Catalunya 35, 43002 Tarragona, Spain² Institut Català de Paleoeologia Humana i Evolució Social (IPHES-CERCA), Zona Educacional 4, Campus Sescelades URV (Edifici W3), 43007 Tarragona, Spain* Correspondence: gustavodaniel.mh@gmail.com; Tel.: +34-689-48-99-32

† These authors contributed equally to this work.

Abstract: The Ndotu cranium is a partial, fragmented, and distorted hominin specimen from the Lake Ndotu site in Tanzania. It was first reconstructed by R. J. Clarke in 1976 and later revisited using now-outdated techniques. Consequently, features such as facial projection, cranial height/length, and cranial flexion are contestable. Here, we present a new virtual reconstruction following a transparent and replicable approach that employs virtual anthropology techniques to reassemble, mirror, digitally align, complete the cranium, and remove the effect of plastic deformation. Before deciding on an approach to align the unarticulated fragments, we tested the effects of symmetrization and the use of surface semilandmarks on the performance of our tool of choice: the digital alignment tool (DTA), developed by A. Profico and colleagues in 2019. Upon completion, we compare our reconstruction to a sample of Pleistocene hominin crania via geometric morphometrics. Test results reveal that DTA performance varies by fragment and that the use of surface semilandmarks bears no statistically significant advantage. We found our reconstruction to boast a more prognate and narrower face with a less flexed cranium overall than previous reconstruction efforts. The shape of the reconstructed cranial vault of Ndotu resulted closest to Sima de los Huesos (SH) 5, while its sagittal profile was most similar to Kabwe's, lending support to J. L. Arsuaga and colleagues' 1997 work and to P. Rightmire's, respectively. We warn that further work is necessary before settling the debate surrounding Ndotu's phylogeny. However, if our reconstruction hypothesis is held, its inclusion in future morphological studies is granted.



Citation: Montiel, G.; Lorenzo, C. A New Virtual Reconstruction of the Ndotu Cranium. *Heritage* **2023**, *6*, 2822–2850. <https://doi.org/10.3390/heritage6030151>

Academic Editors: Gizeh Rangel-de Lazaro and Adrián Martínez Fernández

Received: 28 December 2022

Revised: 22 February 2023

Accepted: 5 March 2023

Published: 9 March 2023



Copyright: © 2023 by the authors. Licensee MDPI, Basel, Switzerland. This article is an open access article distributed under the terms and conditions of the Creative Commons Attribution (CC BY) license (<https://creativecommons.org/licenses/by/4.0/>).

Keywords: Ndotu; virtual reconstruction; human evolution

1. Introduction

The Ndotu cranium was discovered in late 1973 by Amini Mturi, director of Antiquities of Tanzania, at the western end of the Oldupai Gorge, in the sediments of a seasonal soda lake, called Lake Ndotu. Mturi aimed to determine the stratigraphic origin of artifacts and fossils assigned to the Upper Acheulean that had been found along the western shore of the lake during the dry season, when he stumbled upon human fossils. The Ndotu cranium rested aside some fragments of faunal remains, embedded in a subunit of silty clay in the shallower of two archaeological horizons. At the upper limit of the unit to which these strata belonged rested a reworked tuff that today has been correlated with the Norkilili member of the upper part of the Masek beds of the Gorge, dated at 450 ± 40 Ka BP [1,2].

After millennia of being subject to the cycles that affected the lake sediments that enclosed it, the cranium was considerably fragmented and distorted. Large sectors of the face and cranial vault had been completely lost. The salt had penetrated the diploe and had been dissolving and recrystallizing during the wet and dry periods, in many cases, separating both tables of compact bone. This process had left the parietal bones dilated (exaggeratedly thick) or without their internal or external tables. A substantial deformation in the anterolateral portion of these bones was also evident.

Much of the antero-superior end of both parietals had disappeared and so had most of the frontal bone. From the splanchnocranium, only the circumnasal area, the medial wall of the right orbit, and the anterior part of the left maxilla were preserved. No teeth were recovered from the site, although a few roots were present. On the other hand, most of the occipital was preserved. Most of the scale and the mastoid portions of the temporals were in good condition, although the petrous portion of the left temporal was fragmented.

The specimen and its surrounding sandy clay matrix were extracted from the site and, in February 1974, they were handed over to Ronald J. Clarke in Nairobi, where he began work on the reconstruction. Clarke restored the position of the constituent fragments and reconstructed the missing parts with gypsum plaster. Although at that time there was no knowledge of the presence of a supraorbital torus, Clarke sensed that there should be, and sculpted it in plaster.

Clarke published the results of his work, along with his morphological analysis, in *Nature* in 1976. Although he acknowledged that it possessed some derived characteristics, his description associated the cranium with a new subspecies of *Homo* (hereinafter *H.*) *erectus*. He argued that the fossil resembled those attributed to *H. erectus pekinensis* in its outline (seen in vertical norm), in the overall shape of the occipital bone, and that of its mastoid region, as well as in the presence of a vault of marked thickness with a pronounced frontal slope. However, he clearly denoted the prominent parietal bossing of the cranium, the existence of an ossified styloid process, and the absence of both a sagittal keel and an extended supramastoid crest reaching the acoustic meatus as *sapiens*-like.

However, not long after, in August 1978, Clarke reconsidered his reconstruction. Three additional fragments had been found after classifying the remains of fauna recovered in 1973. The fragments included a left frontoparietal fragment that articulated with the rest of the calvary, a fragment of the left supraorbital torus that did not articulate from the frontal bone, and a degraded parietal fragment that did not clearly fit anywhere. The new fragments were added to the reconstruction, and the preserved parts of the facial skeleton were repositioned to make room for these additions. Clarke warned that: “[the position of the facial fragments] *should be considered only as a reasonable approximation*” [3] (p. 707).

In 1990, Clarke published a revised description in the *Journal of Human Evolution*, where he made sure to respond to some researchers who had been quick to express their opinion on the 1976 reconstruction. On this occasion, he compared the Ndutu cranium with several specimens, including Salé, O. H. 9, KNM ER 3733, SK 847, and Steinheim. He also elaborated craniograms and compared them with those made by Weidenreich in 1943 using Zhoukoudian XII. Finally, he expanded his interpretation of the phylogeny of the specimen.

Like Clarke, [4], G. Philip Rightmire noticed that the prominence of temporomandibular articular eminence and the postglenoid process, the thinness of the inferior tympanic border, and the characteristics of the styloid process also linked the Ndutu to a sub-Saharan variety *H. sapiens*. Therefore, Rightmire argued that this specimen should be attributed to a female of a subspecies within that taxon, perhaps a “*H. sapiens rhodesiensis*”. However, in 1990, Clarke disputed that, considering the traits observed in SK 847 and O.H. 9, only an elevated anterior articular eminence suggested a link to modern humans. Rightmire also argued that the degree of parietal bossing, as reconstructed by Clarke in 1974, could have been exaggerated. However, Clarke replied that it was reasonable given the similarities of the cranium to Salé’s specimen.

Clarke had found striking similarities between the Specimens of Salé and Ndutu, both in size and shape (again, in vertical norm, but also from behind, due to their parietal bosses), added to a possibly corresponding geological age. Like Ndutu, Salé lacked a sagittal keel, had a short, deep glenoid fossa, an ossified styloid process, and a similar supramastoid region. Unfortunately, later publications would undermine this argument, given the observation of signs of pathology in Salé’s cranium [5].

Considering the morphology observed in O. H. 9 and KNM ER 3733, Clarke retracted his claim that the absence of a sagittal torus and the presence of a short supramastoid crest

linked Ndutu to *H. sapiens*. He found that the only complex of *sapiens* traits that was absent from both *H. erectus pekinensis* and *H. erectus* was the least pronounced occipital–nuchal angle, along with a downward-facing occipital plane, and (again) the parietal bosses.

Clarke, however, agreed with many of the arguments put forward by Rightmire, as well as with some of Bräuer’s statements (1984 in Clarke [3]). He noted that their disagreement was essentially a matter of deciding to assign the Ndutu specimen, which lies somewhere between *H. erectus* and *H. sapiens*, to either an evolved version of the former or an archaic form of the latter.

Although he had defended the first arrangement in his 1976 publication, Clarke would now opt for the second one, namely that Ndutu belonged to a “representative of archaic *Homo sapiens*” [3] (p. 727). For him, the specimen was within the range of the cranial morphotype of the specimens of Salé and Steinheim, a group that he considered different from that formed by Bodo, Kabwe, Saldanha, and Petralona (which, for many researchers, were synonymous with *H. heidelbergensis* or *H. rhodesiensis*). He also deemed it distinct from others, including the fossils of Florisbad, Omo 2, and Ngalooba. Subsequently, he suggested that such a morphotype could in fact derive from an early African lineage, different from the one that must have led to the Asian *H. erectus* (which included *H. erectus pekinensis*). In addition, he postulated that this ancestral lineage, for which he proposed the name *H. leakeyi*, developed a distinctive technological repertoire (i.e., the Acheulean) and remained west of the Movius line.

Clarke’s interpretations of the Ndutu cranium’s place among the diversity of Middle and Late Pleistocene hominids and their role in the evolution of *H. sapiens* have been discussed more recently by other authors. In 1997, Arsuaga, Martínez, Gracia, and Lorenzo added their perspective to this discussion. They published a lengthy article concerning the affinities of a collection of recently discovered early European hominin crania. The group of specimens recovered by the team from the Sima de los Huesos deep vertical shaft in the Sierra de Atapuerca (Northern Spain) have been interpreted as akin to an ancestor of the Neanderthal lineage [6]. One metric study among the long series of comparative analyses put forth to justify their conclusions featured the Ndutu cranium. It considered eight metric variables from the occipitals of a sample of Middle and Late Pleistocene hominins. These variables described a considerable portion of the occipital morphology, including the occipital curvature, the occipital angle, and the inion–opisthion chord. In a PCA of these variables, the Ndutu cranium also proved to be similar to the very complete SH cranium 5, although it was closer to the Steinheim, Tabun 1, and Zhoukoudian XI fossils.

Likewise, in light of new emerging data, including the affinities of the SH hominins, alongside new dates and morphometric and genetic studies, while reviewing the state of the relationships between specimens in the Middle to Late Pleistocene human fossil record, Chris Stringer [7] also extended his opinion on Ndutu’s phylogeny. Advancing the results in [8], he presented *H. heidelbergensis* as a European branch of Neanderthal descent, but unrelated to the fossils that led to *H. sapiens*. Regarding the taxonomy of the Ndutu cranium, Stringer decided on an arrangement like Clarke’s. While Stringer dismissed the Steinheim cranium as more akin to the Neanderthal lineage, he contemplated that specimens such as Ndutu, along with the Thomas quarry mandible, could better fit into an archaic form of *H. sapiens*. On the other hand, the morphotype of Bodo and Kabwe would then constitute a separate group, closer to the Neanderthal lineage.

The following year, Rightmire published his own discussion of Middle and Late Pleistocene hominids, insisting on a different arrangement for Ndutu. In this article, the author reflected on the temporal and regional morphological differences between these hominins and the relevance of this for their taxonomy. It took into consideration the relative size of the brain, the globular shape of the cranial vault, the thickness of the supraorbital torus, postorbital constriction, parietal expansion, occipital angulation, occipital scale shape, and facial proportions. Rightmire pondered the variation of these measurements within and between groups of hominin fossils or “paleo-demes” that he built based on the temporality

and location of their discovery. Here, he emphasized the morphological similarities that he considered indicative of their affinity.

In [9], Rightmire presented his interpretation of the evolutionary path to anatomical modernity. Like Tattersall and Schwartz (2008 in Rightmire [9]), he envisioned the *sapiens* trait complex emerging at a distinctive point in time through a process of speciation. In the end, while acknowledging that some traits such as cranial globularity and postorbital constriction seem to advance gradually, Rightmire assigned most of the specimens he examined to *H. sapiens*, except for a handful, including Ndutu.

In his view, the Ndutu cranium, alongside Bodo, Kabwe, Saldanha, Zuttiyeh, and Omo 2, exists outside the *sapiens* range. Specimens of this group are characterized by having lower and wider cranial vaults than those of Florisbad, LH 18, KNM-ER 3884, Omo 1, Djebel Irhoud, Herto, Singa, and Aduma (although not later Levantine fossils, such as that of Skhul V). They also exhibit relatively low endocranial volumes and high postorbital constriction. Finally, they have massive supraorbital tori, along with a correspondingly high degree of facial projection. Rightmire specifies that the appropriate designation for the Ndutu cranium and similar fossils should be *H. heidelbergensis* or “some closely related species restricted to Africa” [9] (p. 16048)—that is, *H. rhodesiensis*, if the specimen from the Zuttiyeh cave is excluded.

In the current state of affairs, contrasting hypotheses regarding the position of the Ndutu cranium among the various human fossil exemplars of the Middle and Late Pleistocene coexist. Most of the latest efforts in this regard are particularly preoccupied with its relationship to the Kabwe and Bodo specimens and, consequentially, Ndutu’s affinity with *H. heidelbergensis*.

However, unlike the exquisitely preserved Kabwe specimen, the Ndutu fossil is fragmented and distorted. Many significant features have been obscured, at least partially, by its troubled taphonomic history. To make matters worse, there still seems to be no current consensus on what *H. heidelbergensis* signifies [10]. As a result of a thorough discussion on this polemic stemming from a conference session at the American Association of Biological Anthropologist’s 2019 annual meeting, Roksandic and colleagues resolved to exclude the Western European exemplars from this ill-defined hypodigm—which they waggishly call “the muddle in the Middle”. They also argue to abandon the *rhodesiensis* nomen because it alludes to the Kabwe specimen, a late survivor of the lineage [8], and it references colonialism. In its place, they employ *H. bodoensis* as the taxonomical designation for a Middle Pleistocene hominin taxon spanning across Africa and the Levant. Here, they also include the Ndutu cranium, although they do not specify any autapomorphisms. Instead, the taxon is diagnosed given the presence of a particular mixture of “*H. erectus-like and H. sapiens-like features*” [10] (p. 25).

Whenever explicitly taken into consideration, Ndutu’s correspondence to any taxon has been settled based on occipital angle and curvature, temporomandibular joint, and supraorbital and zygomaxillary morphology, as well as height and cranial globularity, among other metric and nonmetric traits. While some assign Ndutu to a distinct line that eventually leads to anatomically modern *H. sapiens* on this basis, many researchers do not agree. This is unsurprising given that several features, including postorbital constriction, supraorbital projection, facial projection, prognathism/orthognathism, and cranial flexion, presently remain unclear.

The few observations that some researchers have risked extending regarding such biologically significant traits (e.g., [3,4,7,9]) rely on a reconstruction made using techniques that rely heavily on interpretation, are hard to replicate, and can now be replaced with some that are intelligibly statistical. Furthermore, as related previously, this reconstruction has been criticized for the exaggeration of *sapiens-like* traits, such as the bosses on its parietals. To the best of our knowledge, the occurrence of this feature (asymmetrically present on a pair of heavily fragmented bones known to have been subject to distortion) has not been discussed any further after 1990 in the literature.

Formerly, reassembling broken heritage items, such as fossils, was a tedious and conspicuously error-prone activity. Currently outdated techniques amplified the chance for subjectivity and bias and precluded the documentation of all of the steps undertaken [11]. As a consequence, the last 30 years have seen great advances in the development of techniques aimed at helping and even automating this task by implementing advanced algorithms [12]. Today, manual, assisted, and automated virtual reconstruction methods such as digital crack removal, reflection, element duplication, digital reassembly, and feature estimation and retrodeformation are applied almost routinely. In light of the current widespread availability of these tools, the production of a new digital reconstruction of Ndotu is at hand.

Considering what was discussed in the previous paragraphs, improving our understanding of the spatial relationships between the fragments that make up the Ndotu specimen, its distorted and missing anatomy is key to improving our current interpretation regarding its phylogeny. The implementation of informatic resources in this matter promises new insight into Ndotu's contended features. The statistical interpolation of the cranium's features, as facilitated by electronic means, should allow to complete at least some of the portions of Ndotu's anatomy missing from previous reconstructions and correct the distortion affecting its parietals, thus granting its inclusion in a greater volume of shape-based morphological studies.

Thus, our goal is to create a novel morphological hypothesis of Ndotu that, unlike Clarke's, has an explicit statistical basis. We aim to provide the paleoanthropological community with a new virtual reconstruction which will help settle the debate of Ndotu's phylogeny in the future.

2. Materials and Methods

In its current state, the Ndotu cranium is a fragmented human fossil comprised of various continuous and discontinuous fragments. In the following lines, we provide a description of this specimen, which was the main substrate of this work.

- **Facial skeleton and dentition**

In its present condition, the Ndotu cranium's face is represented by a disarticulated piece held in place with a generous amount of gypsum plaster. It gathers most of the maxillary bone, the antero-inferior portion of the zygomatic root, the greater part of the right lacrimal bone, and most of both nasals, as well as a small, attached fragment of the ethmoid representing the crista galli [3]. More accurately described as a near-continuous cluster of fragments, this piece boasts a flat midfacial region [13]. Here, the preserved nasal aperture opens tall and moderately wide, flanked by thin nasal margins. Above it, the inferior two thirds of the nasals sharply angle down and outward. To the sides, the orbital margins also slope infero-laterally quite markedly. On the better-preserved right side, this slope can be seen to yield above the infraorbital foramen [3]. Crispily defined lacrimal crests delimit tall and narrow lacrimal fossae [13].

The inferior nasal margin is mostly missing, as so is the incisor portion. The left anterior part of the palate reveals a deep curve, to the side of which only a part of the left dental arcade from C1 TO M1 is present [3]. To Schwartz and Tattersall [13], the C1 root appears short, while the distance between the buccal and lingual roots of M1 seems long. Both premolars are double-rooted.

- **Frontal bone**

The frontal bone is represented by a detached left fragment of the supraorbital torus (most of which has been sculpted in plaster) and two frontal squama fragments that articulate with the parietals on either side of the cranial vault. Although the temporal crest is mostly visible on the left supraorbital torus fragment [3], its root can also be distinguished on the right frontal fragment, close to the orbit on its broken end. Overall, these lines are sharp and extremely low, allowing for a steep frontal rise that may be argued to be even more precipitous than estimated by Clarke [13].

For its part, the anterior part of the left temporal line on the supraorbital torus fragment's reverse is well-preserved from its departure close to the fronto-zygomatic suture to what is likely beyond the point of minimum frontal breadth. Furthermore, the left supraorbital torus fragment is shown in Clarke's latest reconstruction to account for the central and lateral parts of the upper orbital rim and thus shows a piece of the lateral part of the orbital roof. Notably, it boasts a considerably large foramen near its right end.

- **Sphenoid bone**
The preserved sphenoid encompasses the posterior portion of the right orbital surface of the right greater wing forming the roof of the right orbit, as well as a part of the right temporal surface, a smaller piece of the left temporal surface, and a small fragment of the lesser wing. On this area, several small ethmoid fragments were also noted by Clarke [3]. Conspicuously, most of the sphenoid body is missing and many of the inner fragments are disarticulated, which implies a degree of uncertainty in the width of the sphenoid.
- **Parietal bones**
In their current state, the parietals are missing various sections of either their inner or outer tables. Indeed, they constitute the most deteriorated of the preserved parts of the Ndotu cranium, having sustained a great deal of erosion and both plastic and brittle deformation. This particularly affects the anterior part of the right parietal and the posterior end of the sagittal suture, as admitted by Clarke in 1990. Despite this, Clarke's meticulous work allowed to recover what is known about this part of Ndotu's braincase. According to his reconstruction, their parietals are noticeably thick, display a large diploic space, and appear quite bossed—a trait that has been largely exaggerated on the right side by taphonomic deformation. Still, as indicated by the left parietal contour, it can be agreed that the neurocranium would have been rather short, round, and wide [13].
- **Temporal bones**
Both temporals are present, with some of their squamae and at least a hint of the root of both zygomatic processes being preserved. In addition to this, on the right, this is limited to the superior part of the acoustic meatus, the lateral segment of the glenoid fossa, the supramastoid crest, and most of the mastoid portion. Contrastingly, the better-preserved left temporal adds information on this anatomy, plus the presence of a remarkable tympanic plate and the styloid process. Ndotu's temporal squamae project straight upward, supporting a wide neurocranium [4,14] and possibly arching quite high on the sides of the cranial vault. Their temporal anatomy also exhibits a striking articular eminence in front of a short and narrow glenoid fossa. Alongside this are short and stout mastoid processes and a modest occipito-mastoid crest.
- **Occipital bone**
The Ndotu occipital is nearly complete. It is most notably lacking the basilar process and the left occipital condyle, alongside a few squamous fragments. The foramen magnum is ovoid in shape and the condyles seem to have been forwardly positioned. As the squama extends posteriorly, it meets a rather faint occipital torus. Despite this, the occipito-nuchal angle is sharp (110° according to Clarke). On its end, the squama exhibits a moderately sized interparietal bone that, according to Tattersall [13], obscures the position of lambda. Projection of the lambdoid and sagittal sutures locate lambda close to the superior edge of this Wormian bone.

Taking into account its current state, it is clear that, to achieve a new virtual reconstruction of this specimen, several procedures, ranging from fragment mirroring, reassembly, digital alignment, and interpolation of missing data to retrodeformation, were necessary. Similarly imperative were the production of guiding information and the preliminary demonstration of the outcome of our efforts. Thus, with these purposes in mind, we

resorted to a wide array of software packages. We disclose the procedures undertaken and the informatic resources employed to perform them in Table 1.

Table 1. List of procedures undertaken during the virtual reconstruction of the Ndotu cranium and the software employed.

Procedure	Software Package(s)
Segmentation of CT scan data	Materialise Mimics Medical 21.0.0.406
Generation of disarticulated fragment models	MeshLab 2022.02
Photogrammetry of fossil replicas for reference sample	Agisoft Photoscan Professional 1.40 build 5076
Reassembly of articulated fragments of the neurocranium	Fragment Reassembler 1.0
Mirroring of the facial skeleton	MeshLab 2022.02
Landmark digitization	MeshLab 2022.02
Surface semilandmark digitization	R (Morpho, Geomorph, and other packages), MeshLab 2022.02
Digital alignment tool testing	R (Arothron and other packages)
Test results analysis	R (Rstatix, BestNormalize, and other packages)
Alignment of disarticulated fragments	R (Arothron package)
Completion of the Ndotu cranium via interpolation	R (Morpho, Geomorph, and other packages)
Retrodeformation of the anterior fragment of the right parietal	R (Morpho, Geomorph, and other packages)
Comparison with previous reconstruction	R (Morpho, Geomorph, and other packages)
Digitization of curve semilandmarks	3DSlicer 5.2.1 (SlicerMorph)
Shape analysis	R (Morpho, Geomorph, and other packages)

The first step of the reconstruction process was to prepare the 3D models that represent the articulated and disarticulated fragments that constitute our starting rendition of the Ndotu cranium. The creation of said 3D models was possible through segmentation of the CT scans of the original fossil produced by Weber et al. [15] in 1998 and acquired by the Institut Català de Paleocologia Humana i Evolució Social (IPHES-CERCA). Back then, the disassembled Ndotu cranium was scanned in eight parts using a Siemens Somatom Plus 40 CT scanner. We segmented these eight scans and further processed the 3D data to produce eleven distinct 3D models following the procedures detailed in the following paragraphs.

It is noteworthy that some of the 3D models created represented single fragments, while others comprised clusters of several minor articulating fragments. Regardless, they are all generally referred to as “fragments” in this work. For the sake of clarity, Table 2 lists the fragment 3D models obtained after segmentation of the CT scans alongside their identification and whether or not they match any other fragments or are disarticulated according to Clarke [3].

Weber and colleagues’ data [15] encompassed a varying number of 1 mm-thick slices captured with 1 s exposition time using a 512×512 matrix with different pixel sizes and display fields of view (FOV). CT scans No. 1, 3, 4, and 5 (the anterior part of the cranium as assembled by Clarke and the occipital; see Table 2) consisted of 136 slices (each) with a 0.51562×0.51562 mm pixel size and a display FOV of 264, while CT scans No. 2, 6, 7, and 8 comprised 84 slices (each) with a 0.32617×0.32617 mm pixel size and display FOV of 167.

The TIFF-format images of the slices contained in Weber et al. [15] were imported into the Materialise Mimics Medical [16] software. We adjusted the scan resolution parameter to match the pixel size of each CT scan. Once the CT scans were fully loaded in the software, we proceeded with the segmentation process. For each scan, we adjusted the parameters of the Threshold function manually to create eight masks that fit a range between 43,225 and 65,535 GV, as shown in Figure 1. The specified range excluded all other materials except for the fossilized bone. This allowed to digitally remove the gypsum plaster holding the disarticulated facial skeleton and left supraorbital fragments in place in CT scan No. 1.

All of the masks were exported from the Materialise Mimics software in Optimal quality in Stanford’s Triangle (PLY) format. In the case of CT scan No. 1, the “floating” supraorbital and facial fragments of the Ndotu cranium were subsequently separated from the preserved frontal, temporal, and sphenoid and saved as four distinct *.ply files using Cignoni and colleague’s [17] MeshLab software.

Table 2. Fragment number, CT scan number (in Weber et al. [15]), identification, and articulating fragments or fragment clusters of the 3D models of the fragments of the Ndutu cranium obtained via segmentation of CT scan data. Identification and articulated fragment matching based on Clarke [3].

Fragment No.	CT Scan No.	Identification	Articulates with No.
1 ¹	1	Left circum-nasal area, medial wall of the right orbit, and anterior portion of the left palate, with a disarticulated fragment of the right upper lateral border of the nasal aperture.	Disarticulated
2 ¹	1	Left lateral supraorbital.	Disarticulated
3 ¹	1	Right lateral frontal squama and fused lower anterior right parietal, right greater wing of the sphenoid, lower anterior temporal, and a disarticulated fragment of the left lesser wing of the sphenoid.	5, 9
4 ¹	1	Left lateral frontal squama fragments of the upper posterior and (disarticulated) lower posterior lateral surface of the left greater wing of the sphenoid; squamous and mastoid portions of the left temporal.	5, 8
5	2	Left and right parietals (excluding the anterior third of the left one and the antero-medial portion of the right one), including several disarticulated inner and outer tabula fragments.	3, 4, 8, 9
6	3	Distal medial occipital squama including interparietal bone.	5, 7, 8
7	4	Single fragment of the left part of the distal occipital squama.	5, 6, 8
8	5	Restored occipital bone including the nuchal plane, the base of the occipital planum, and the posterior and right lateral borders of the foramen magnum, fused to the mastoid portion of the right temporal.	4, 5, 6, 7, 9, 10
9	6	Right temporal squama	3, 5, 8
10	7	Anterior and left lateral borders of the foramen magnum.	8
11	8	<i>Unmatched</i> parietal fragment cluster.	Disarticulated

¹ Separated in MeshLab after segmentation.

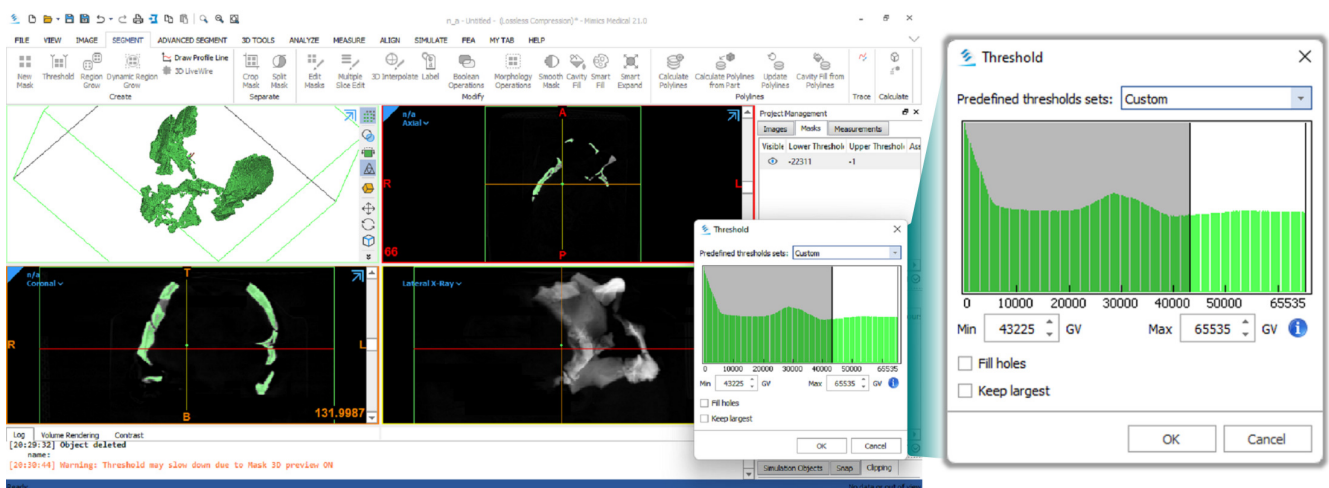


Figure 1. Segmentation of CT scan No. 1. Materialise Mimics 21.0 window showing the green mask, lateral X-ray view, and slices of CT scan No. 1 in simulation view, along with the Threshold dialog box (left). Magnification of the Threshold dialog showing custom GV range (right).

Next, we collected 21 additional 3D models of well-preserved hominin skulls to create a sample to use as a reference during the reconstruction process. Within the bounds of the selection standards related to preservation, we aimed to avoid over-representation. Hence, with the notable exception of the Dmanisi sample (which exhibits a wide morphological variation), we set to select fossil specimens from different sites and/or strata.

Ten of the specimens consisted of replicas found in the Paleoanthropology Laboratory at the IPHES-CERCA in Tarragona, Catalonia. These replicas were digitized using photogrammetry. The replicas were placed on a low table over a white cloth with a 5 cm scale in front of them at the IPHES-CERCA Paleoanthropology Laboratory. Pictures were taken with a Canon EOS 2000D reflex camera at 50 mm focal length, at 1/60 shutter speed, with an indirect light source (the sun and the laboratory's left side lights) during the day. The exposure (ISO) was adjusted between 200 and 400 as necessary to compensate for daylight intensity changes in between specimens. A tripod was used for camera stabilization and positioning. The 34 to 36 captured images were processed in Agisoft Photoscan Professional version 1.40 build 5076 [18].

The rest of the 3D specimens were obtained from personal communications and online repositories. These models were created through several means, ranging from CT scans to laser and structured light scanning. Table 3 summarizes the information regarding the digital capture method, CT scan resolution (if it applies), vertices, faces, specimen type, and source of the specimens in the sample.

To restore the position of the articulated fragments of the Ndotu cranium, we began by searching for accessible automatic and semiautomatic reassembly software that matched the needs of the reassembly at hand. To select suitable software candidates, we considered the requirements imposed on the object to be reassembled, which implies that we took the use of algorithms or procedures tailored to deal both with eroded fragments and with fragment overlap, as well as the implementation of optimization functions, into account. In the end, we selected two software applications: Papaioannou and colleague's [19] PRESIOUS VRMW virtual reassembly system and Palmas and colleague's [20] Fragment Reassembler.

Following the procedure detailed on each reassembly software's publication, we attempted to reconstruct the Ndotu cranial vault and base. While the PRESIOUS VRMW system failed to identify any matching fracture surfaces as promised, the Fragment Reassembler software offered better results. It allowed to execute an assisted reassembly based on the placement of constraints, i.e., points along the opposing surfaces of fractured objects.

The Fragment Reassembler manages the rigid transformations necessary to rotate and translate the 3D models of each fragment pair to minimize the distance between coupled points along the fracture surfaces. Imperfect matches hold more residual energy, which the software minimizes by implementing an overall energy reduction optimization algorithm. With this tool, 3D models are assembled hierarchically by grouping pairs of assembled fragments or fragment groups. However, when a new fragment is matched with a group, energy minimization is not performed across all fragments but only within that group. Therefore, to finish up the process, we deleted the hierarchy and executed the optimization algorithm as indicated in Palmas et al. [20]. The constraints graph in Figure 2 illustrates the reassembly process by showing the hierarchical order in which the articulated fragments of the Ndotu cranial vault and base were reassembled using this software.

For comparative purposes, we later employed the same software to reassemble an alternative version of the entire Ndotu cranium using CT scan No. 1, i.e., Clarke's original facial reconstruction boasting "floating" supraorbital and facial fragments that were still aligned as he had intended. Given that the space between the lateral frontal fragments had remained as far apart as Clarke had placed them, the resulting model exhibited slightly outwardly oriented frontal bones that bestowed upon it a moderately wider frontal region than the newly reassembled cranial vault and base. Figure 3 shows a comparison between the 3D model of the Ndotu cranium having been reassembled using Clarke's original facial reconstruction and our restoration of cranial vault and base having removed the constraints introduced by keeping the spacial relationships between unarticulated fragments as interpreted by Clarke.

Table 3. Name, digital capture method, CT scan resolution, vertices, faces, specimen type, and source of the 3D models in the reference sample.

Specimen Name	Digital Capture	CT Scan Resolution	Vertices	Faces	Specimen Type	Source
Amud 1	Photogrammetry		2,230,885	4,461,770	Replica	Paleoanthropology Laboratory, IPHES-CERCA (own data)
D2282	Photogrammetry		1,498,772	2,996,828	Replica	Paleoanthropology Laboratory, IPHES-CERCA (own data)
D2700	Photogrammetry		1,285,589	2,570,089	Replica	Paleoanthropology Laboratory, IPHES-CERCA (own data)
D4500	Photogrammetry		1,109,845	2,219,686	Replica	Paleoanthropology Laboratory, IPHES-CERCA (own data)
Dali	Laser scan		367,362	732,191	Replica	Muséum National d'Histoire Naturelle
BOU-VP-16/1 (Herto)	Photogrammetry		2,178,417	4,356,086	Replica	Paleoanthropology Laboratory, IPHES-CERCA (own data)
Irhoud 1	Photogrammetry		1,215,368	2,430,726	Replica	Paleoanthropology Laboratory, IPHES-CERCA (own data)
Kabwe	CT scan	x = 0.108868 mm, y = 0.108868 mm, z = 0.108868 mm	1,073,374	2,052,377	Replica	Morphosource.org (Duke University)
KNM ER 1470	Photogrammetry		49,989	100,006	Replica	AfricanFossils.org (Turkana Basin Institute)
KNM ER 1813	Laser scan		49,966	99,928	Replica	AfricanFossils.org (Turkana Basin Institute)
KNM ER 3733	Structured light scan		49,984	99,972	Replica	AfricanFossils.org (Turkana Basin Institute)
La Chapelle-aux-Saints	CT scan	x = 0.123 mm, y = 0.123 mm, z = 0.123 mm	719,164	1,430,560	Original Fossil	Muséum National d'Histoire Naturelle
La Ferrassie 1	Laser scan		648,417	839,550	Replica	Muséum National d'Histoire Naturelle
Lesedi 1	Laser scan		1,944,690	3,889,412	Original Fossil	Morphosource.org (University of the Witwatersrand)
Sima de los Huesos 5	Photogrammetry		1,418,721	2,837,354	Replica	Paleoanthropology Laboratory, IPHES-CERCA (own data)
Mladeč 1	CT scan	x = 0.4668 mm, y = 0.4668 mm, z = 0.75 mm	234,610	468,560	Original Fossil	Natural History Museum Vienna
Petralona 1	Photogrammetry		1,821,546	3,640,857	Replica	Paleoanthropology Laboratory, IPHES-CERCA (own data)
Qafzeh 9	Photogrammetry		1,648,506	3,296,880	Replica	Paleoanthropology Laboratory, IPHES-CERCA (own data)
Sangiran 17	CT scan	x = 0.107417 mm, y = 0.107417 mm, z = 0.107417 mm	1,498,652	2,953,295	Replica	Morphosource.org (Duke University)
Shanidar 1	Photogrammetry		1,741,950	3,488,595	Replica	Paleoanthropology Laboratory, IPHES-CERCA (own data)
Skhul 5	CT scan	x = 0.488281 mm, y = 0.488281 mm, z = 0.5 mm	642,964	1,279,624	Original Fossil	Peabody Museum (Harvard University)
Zhoukoudian XII	Photogrammetry		184,371	386,742	Replica	Paleoanthropology Laboratory, IPHES-CERCA (own data)

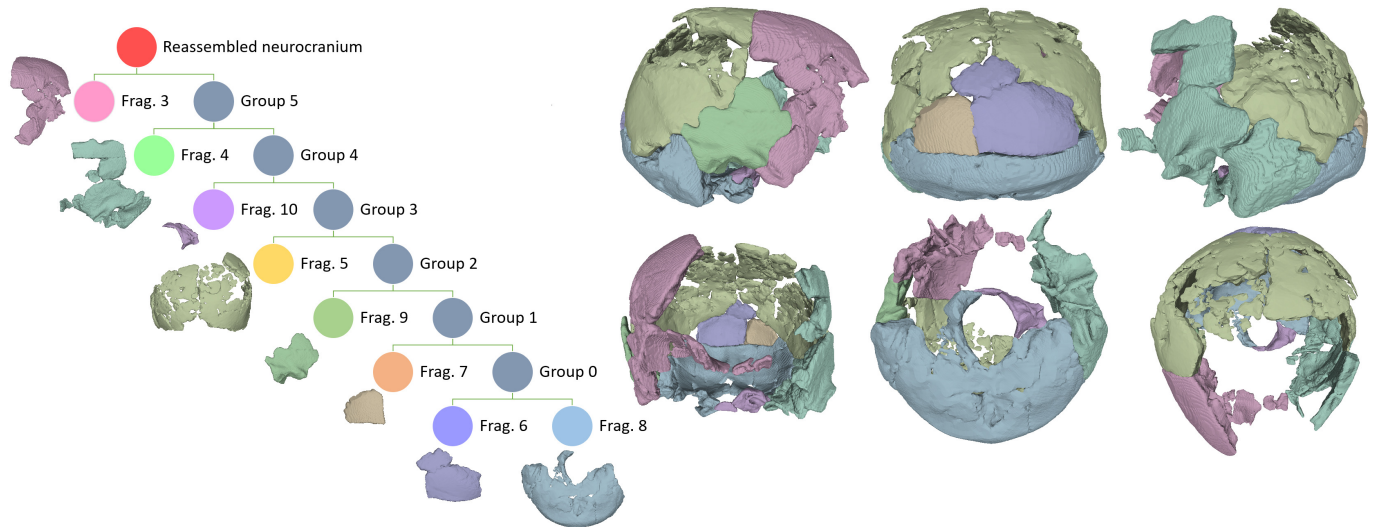


Figure 2. Constrains graph for the reassembly of the Ndutu neurocranial fragment cluster (left) and reassembled model (right, multiple views). Fragments numbered as in Table 2, column 1. Fragments not scaled.

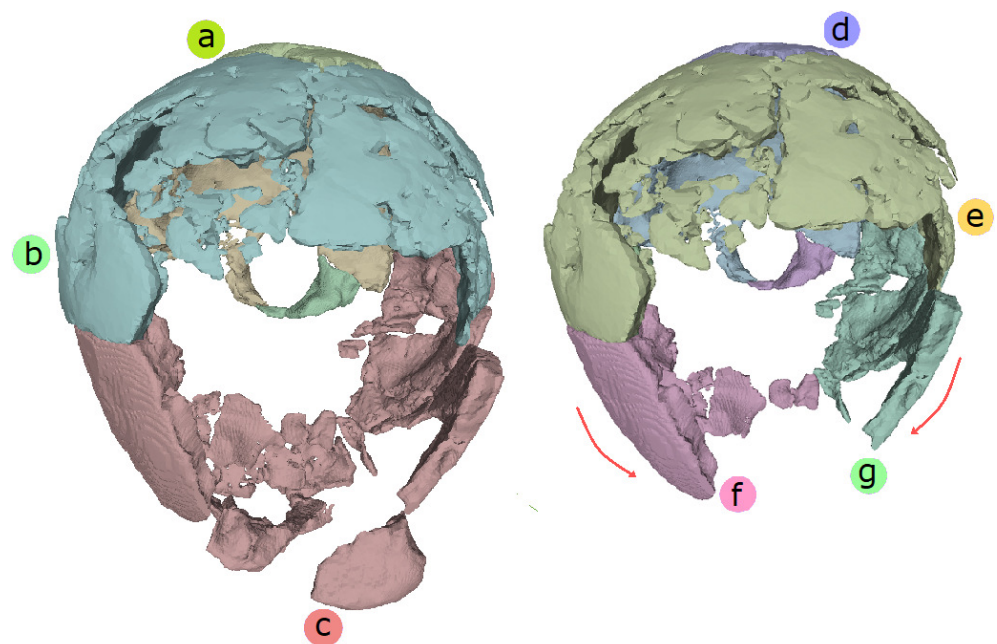


Figure 3. Recreation of Clarke's reconstruction (left) and (right) reassembled Ndutu neurocranium, vertical view. (a,d): Fragment No. 6 (occipital squama and interparietal bone). (b,e): Fragment No. 5 (left and right parietals). (c): Left and right fragments of the frontal, temporals, and anterior parietals, sphenoid, ethmoid, facial skeleton, and left supraorbital, assembled as in Clarke, 1990 (from CT scan No. 1). (f): Fragment No. 3 (clustered fragments of the right hemifrontal, temporal, and anterior parietal, plus right sphenoid wing and body). (g): Fragment No. 4 (clustered fragments of the left hemifrontal, temporal, and anterior parietal, plus left sphenoid wing). Fragments numbered as in Table 2, column 1. Red arrows indicate narrowing of the anterior frontal bone diameter.

Once the Ndutu cranial vault and base were reassembled, we proceeded to realign the disarticulated facial fragments. This time, the “Digital Alignment Tool” (DTA) tool developed by Profico et al. [21] was selected as the main instrument to meet this goal. This software allows to find the best alignment between two portions of a disarticulated model (DM), represented by two different 3D models corresponding to two fragments of the same individual. To do this, it uses a reference model (RM) that is selected from a

sample using a methodology based on geometric morphometrics (GM). For this to happen, the Cartesian coordinates of a common set of “landmarks” are recorded by an expert operator both in the DM and in a reference sample [21]. The single specimen to become the template is selected from the sample based on how similar its landmarks configuration is to that of each of the fragments of the DM. The transformation of the matrix necessary to rigidly rotate and translate the reference matrices of both fragments is handled by the software through a general Procrustes analysis (GPA), which allows to contrast object shapes through superimposition [22,23].

Hence, we constructed a 48 fixed landmark set, which was based on the craniometric points observable in the preserved parts of the Ndutu cranium. Such landmarks were defined as in [24–28] (see Supplementary Information Table S1). We tailored this set to accommodate the largest number of observations possible. Therefore, a few anatomical points present in Ndutu, but not preserved across most of the sample, were ultimately excluded.

The DTA is a versatile tool that also allows to perform an optional symmetrization procedure that reduces the alignment error introduced by asymmetry. Whenever employing a landmark set composed exclusively by paired bilateral landmarks and single midline landmarks, this process creates a symmetrical configuration by reflecting and relabeling the data. Regarding the problem at hand, given the nature of the face and the neurocranium, settling on the convenience of this approach was straightforward.

We then resolved that the only two viable approaches to exploit symmetry for the purpose of aligning the fragments were either to ignore the anatomical details that had been asymmetrically preserved or to mirror the fossils. For the neurocranium, ignoring a few landmark candidates still resulted in a reasonably large and comprehensive landmark set. Yet, for the facial skeleton, we opted to produce a mirrored version of it. This way, we reconstructed the necessary information missing in the Ndutu dental arcade by exploiting bilateral symmetry [11]. A version of the Ndutu facial skeleton mirrored along the mid-sagittal plane was created using the functions in the MeshLab software [17] (Figure 4). To this aim, we duplicated the model, flipped it on its axes, inverted the faces orientation and, finally, realigned it with the original using the Align function in that software—a procedure that, in this case, prevented the need to manually position the mirrored elements.

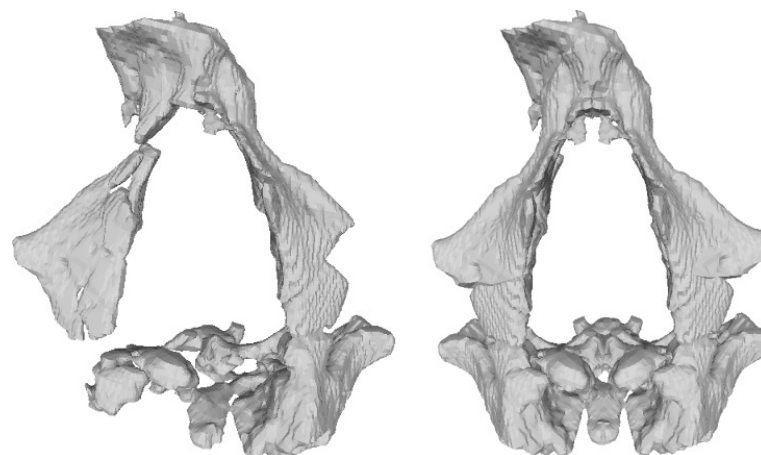


Figure 4. Original Ndutu facial skeleton fragment (left) and mirrored version (right).

Aiming to recover as much information as possible from the damaged and fragmented Ndutu specimen, we recognized that our approach to landmarking disregarded the biologically significant morphological information found on the surfaces of the cranial vault squamae. Furthermore, it entailed the loss of information in the spaces in between the landmarks in the fixed set [29–33] and prevented adequate coverage [34,35]. Thus, arbitrary numbers of sliding semilandmarks were added on demand (roughly the same amount as the fixed landmarks sample on each fragment).

A precedent of this was set in Profico and colleague's publication, where they presented four alternative digital reconstructions of the incomplete skull of *H. neanderthalensis*, known as Amud 1, which is also missing a large part of its facial skeleton. These alternatives resulted from the combination of two different templates, namely the La Ferrasie 1 and Shanidar 1 skulls, and two landmarking approaches. The first of these approaches consisted of using a small set of fixed landmarks. In the second, these landmarks were complemented by surface semilandmarks, that is, several of evenly placed, repositionable points that made it possible to sample the complex surfaces and curves observed along the fossil.

Noticing the possibility that the implementation of semilandmarks and the use of the symmetrization procedure could interact (perhaps even disruptively), we first ran a series of tests on the only fragment pair that could be subject to symmetry constraints—the facial skeleton and the neurocranium. Then, we measured the effect of applying surface semilandmarks on the performance of the DTA on the rest of the fragments. These tests additionally provided us with a measurement of the performance of our tool of choice and our decisions. The procedure detailed in the following paragraphs outputted the mean of the Euclidean distance between the corresponding landmarks in the realigned and original versions of each specimen in our sample (hereafter dubbed “alignment error”). For these purposes, we constructed a large R script capable of managing the data, running the DTA tool iteratively under different conditions, and performing the first stages of analysis.

During the testing rounds, for each one of the specimens in the sample, the script divided the landmark data into three different arrays, one for each of the unarticulated clusters that make up the Ndotu cranium. This allowed to simulate that each specimen of the sample had been broken into the exact same disarticulated fragments as Ndotu had been split by the taphonomic process. Furthermore, it also allowed to use a strictly symmetrical landmark set to align the facial skeleton with the neurocranium, while using an asymmetrical one to align the supraorbital. For each of the two possible array pairs, the DTA was permitted to run. As a result, the tool “realigned” each of the landmark matrices of each specimen as if they were Ndotu's.

In a subsequent cycle, a 3D model of the surface of the preserved portions of the frontal, temporal, parietal, and occipital squamae of the Ndotu cranium was used to create a template with which to apply several surface semilandmarks on the sample's neurocranial squamae. This model was created by using the Paint tool in the MeshLab software [17] to select the outer faces of the polygon representing the Ndotu neurocranium.

Whenever the DTA was executed using surface semilandmarks, the additional landmarks were deleted from both matrices, rendering the length of each array the same as the ones in the prior testing cycle. Each new matrix was later compared with its original version. To do this, the script first eliminated most of the variation derived from the rotation produced by the tool by executing a Procrustes superimposition procedure on both versions of the same specimen. Then, it calculated the mean Euclidean distance between the landmarks of both specimens.

The data from both alignments (landmarks corresponding to the left supraorbital fragment with those of the cranial vault and base cluster, as well as the landmarks from the facial skeleton with the ones from the cranial vault and base) resulting from both cycles of implementation of the tool were used to create four distributions of reconstructions, with each datum corresponding to the average landmark displacement caused by the DTA (i.e., the mean distance between the original and “realigned” landmark coordinates in cm) in each specimen. Tables providing further detail on the DTA performance tests can be found in the Supplementary Information Document, Tables S2–S12. However, we summarize our findings in the following paragraphs.

Descriptive statistics of the data in each set revealed some information about the performance of Profico and colleagues' tool under distinct conditions. Yet, to better ponder the effects of the use of semilandmarks on the alignment of a given pair of fragments, we aimed to run a two-factorial analysis of variance (ANOVA) test, following a 2×2 design.

Given that analysis results are only reliable when the data meet certain assumptions [36], the normality of the data was tested via the Shapiro–Wilk test, while the homogeneity of the variances (i.e., homoscedasticity) was tested using the Levene test prior to the execution of the ANOVA series. Whenever necessary, the data were transformed to comply with these assumptions. An appropriate transformation was selected by using of the `bestNormalize()` function of the homonymous R package developed by Peterson [37].

Based on the results of these analyses (see Section 3), we settled on aligning the constituting fragments of the Ndutu cranium via a two-step procedure. In the first step, the mirrored facial skeleton fragment and the neurocranium were aligned using the landmarks in the symmetrical set employing the DTA’s optional symmetrization procedure. Subsequently, the resulting aligned model (AM) and landmark matrix was exported from the R environment, and the right fronto-temporale landmark, which would have otherwise prevented the symmetrization procedure from executing on a symmetrical landmark set, was digitized on the partial reconstruction in MeshLab. The data were then returned to R to execute the script for a second time. This allowed to align the left supraorbital fragment.

Once a new estimation of the position of the disarticulated fragments of the cranium was derived, the following step was to interpolate the missing morphological information. As mentioned before, Clarke, like his forerunners, employed plaster to sculpt his hypotheses regarding the missing anatomy of the Ndutu individual. We decided to use well-established GM procedures in our pursuit of this same intent.

To this aim, we set to interpolate a 10,000-point cloud with which to create 3D model of the missing parts of the Ndutu cranium. We began by elaborating a 3D model of the surface of the AM resulting from the previous procedure by resorting to the Paint tool in the MeshLab software in a similar fashion as we carried out during the testing phase of this project. The surface model, which encompassed the surfaces of the aligned neurocranium, facial skeleton, and left supraorbital of the Ndutu cranium, was then used as a template to digitize the corresponding surfaces of the specimens in the reference sample via the application of 45 surface semilandmarks.

Subsequently, we digitized the entirety of the fossil crania in the sample while placing the recently generated data frame containing the semilandmark arrays in the “fixed =” argument of the `digitsurface()` function in Adam et al’s [38] “geomorph” package. To create a point cloud of the desired size based on the morphological information from the anatomy in the sample specimens that corresponded to the areas missing in the Ndutu cranium, we digitized 10,000 new surface semilandmarks.

Afterwards, we created another array where the Ndutu cranium’s landmark configuration was included to exploit the thin-plate spline (TPS) to perform the interpolation. The result was a 10,060-long array. Instead of warping another specimen’s mesh to the interpolated configuration, the `mesh3d()` and `mesh2ply()` functions of the Morpho package were used to turn the array into a .ply file containing a point cloud. The file was opened in the MeshLab software where normals were computed and a polygonal surface was constructed via the Screened Poisson function. This allowed to create a smooth 3D mesh based strictly on the TPS interpolation. Final touches, such as the elimination of a few artifacts resulting from this procedure, were undertaken in the Stitching Blender Foundation’s Blender software [39].

Having the new interpolated cranial vault surface as a base, we set to correct the plastic deformation of the anterior portion of the right parietal noticed by Rightmire in [4] and admitted by Clarke in [3]. We placed semilandmarks on the surface of the AM, and then we digitized the same points on the model where we had interpolated the missing cranial surface using the TPS. We separated the single fragment of the anterior portion of the right parietal that protruded from that side of the cranial vault (Figure 5) of the AM in MeshLab. We then warped the parietal fragment using both semilandmark configurations we had obtained in the previous step. As the warped fragment model was consequently displaced with respect to the origin, we used the Fragment Reassembler software once

again to correctly position it by placing matching points along the surface of another large frontal bone fragment that was already present on the right side of the AM.

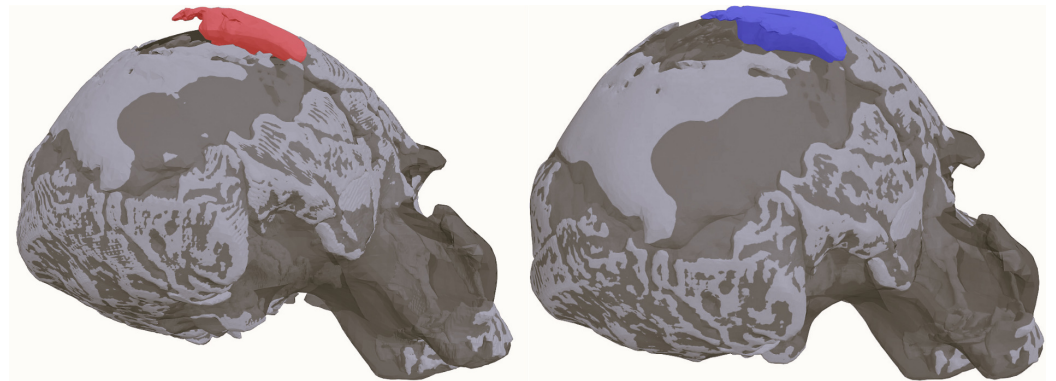


Figure 5. Retrodeformation of the anterior right parietal fragment. Oblique view of the aligned Ndotu cranium with interpolated surface added to show the divergence of the displaced and distorted fragment from the TPS interpolation (**left**); oblique view of the new virtual reconstruction of the Ndotu cranium showing the retrodeformed fragment in the anterior right parietal (**right**).

Once all the fragment-related procedures were undertaken, we simply imported the AM mesh into the MeshLab environment alongside the clean hypothetical surface mesh to then merge both 3D models to create a composite. The resulting model contained the mirrored, assembled, aligned, and retrodeformed fragments of the Ndotu cranium, (including their internal morphology) and the reconstructed surface.

Then, we explored the consequences of the realignment procedure that was accomplished following well-established GM-based morphological comparison methods. With this aim, we set out to compare our reconstruction with Clarke's work and explore the differences between our version of Ndotu and the rest of the hominin sample.

First, a subset of our our fixed landmark set was used to create a TPS deformation grid to visualize the differences between Clarke's reconstruction of the Ndotu cranium and ours. Then, we created two new landmark subsets, one composed of exclusively midline landmarks and another containing only the craniometric points found on the neurocranium.

The sagittal profile landmarks were complemented with a sliding semilandmarks curve created for Ndotu in the 3D Slicer software [40,41] and later digitized on the sample in R. This set allowed to discern traits such as cranial flexion, facial projection, supraorbital protrusion, and relative facial height, as well as cranial height and length.

On the other hand, for a comparison of Ndotu's cranial vault and the sample's own, the landmark set was accompanied with 20 surface semilandmarks digitized on the frontal, temporal, parietal, and occipital squamae of the specimens. This included the retrodeformed and interpolated surfaces.

A Procrustes superimposition was followed by a principal component analysis (PCA) [35]. This made visualizing the variation in terms of shape (the geometric configuration remaining after superposition) between the specimens of a sample possible [35]. Two PCAs were performed subsequently to study the differences between our reconstruction and the hominin sample at hand. Here, sliding curve and surface semilandmarks were utilized Bookstein [30]. The output of this process was two scatter plots that compared two of the components responsible for the largest proportion of the variation in each study, describing a morphospace (that is, a plane that relates and describes the shape of our specimens [42]).

3. Results

3.1. Reassembly

As mentioned in the previous section, the main result of the systematic review performed was the selection of two automatic and semiautomatic reassembly software: Papaioannou and colleague's [19] PRESIOUS VRMW virtual reassembly system, version 1.0, and Palmas and colleague's [20] Fragment Reassembler, version 1.0. Despite its promising approach, due to the extensive erosion of the Ndutu cranial fragments (which had been underestimated by the authors), the PRESIOUS VRMW system was not able to automatically discern neither the borders nor the identity of the fracture surfaces in each fragment using its segmentation algorithm (see Papaioannou et al. [19]), even when the settings were manipulated as indicated by the software's manual. No degree of intervention by the operator allowed it to properly match corresponding fracture surfaces either, given that the segmented surfaces often exceeded the extent of the fractures as discerned by the user. There were also no obvious lines in the fragments that would allow to inform the software and aid the reassembly. Consequently, we were obligated to desist in attempting to reassemble the fragment using this software.

The Fragment Reassembler software outputted much better results. The semiautomatic procedure allowed to match the corresponding fracture surfaces with ease (this correspondence being distinguished by the user via straightforward implementation of anatomical knowledge). The fragments were matched following a hierarchical procedure (see Figure 2) to produce a preliminary reassembly. Once all the vectors connecting all the matched fragment surfaces were introduced in the software, the hierarchy was removed to allow it to perform a global optimization of the reassembly by means of an energy reduction algorithm, as in Palmas et al. [20].

3.2. Digital Alignment

As detailed before, we investigated the possibility of an interaction between the use of surface semilandmarks and the operation of the symmetrization procedure (Figure 6). Descriptive statistics suggested that the highest mean landmark displacement across specimens was obtained upon combination of the consideration of symmetry and the implementation of surface semilandmarks (mean = 0.61 cm, sd = 0.248). Still, omitting the use of surface semilandmarks, while defining landmark pairs, produced only slightly more consistent results (0.165 sd) and marginally better outcomes (mean = 0.452 cm) than avoiding both of these "tweaks" (mean = 0.454 cm, sd = 0.194). The results of the test where only the use of semilandmarks modified the script's regular execution also bear a greater mean displacement with highly variable alignment errors (0.553 sd).

Nevertheless, upon analysis via a two-way ANOVA, it was revealed using semilandmarks was the sole option with a statistically significant influence on the facial skeleton alignment. It had by far the largest effect size ($ges = 0.069$; see Table 4). This made it clear that further testing was necessary.

Table 4. Two-factor analysis of variance (type II tests) of the mean Euclidean distance estimated with and without using surface semilandmarks and with and without symmetrization.

Effect	DFn	DFd	F Statistic	p Value	Ges
semilandmarks	1	80	5.945	0.017 ¹	0.069
symmetry	1	80	0.824	0.367	0.010
semilandmarks:symmetry	1	80	0.906	0.344	0.011

¹ Statistically significant.

The outcome of the second round of DTA performance tests (Figure 7) was mixed. The results varied per aligned fragment, indicating that the same approach harbored different levels of accuracy for different sets of landmarks. Furthermore, as presented in Tables 5 and 6, applying surface semilandmarks did not bear a considerably higher degree of accuracy.

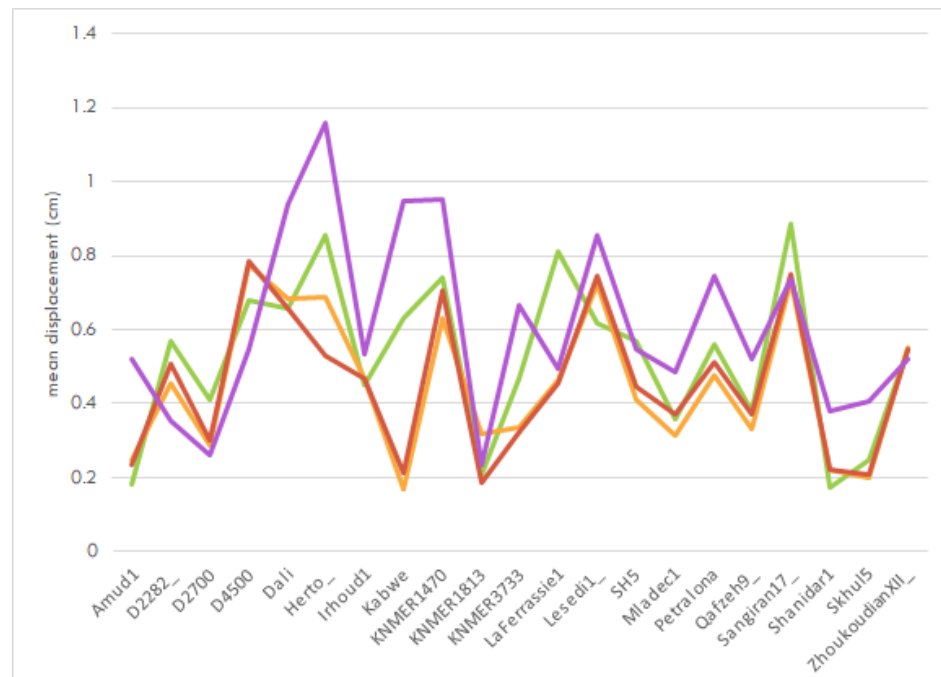


Figure 6. Mean Euclidean distance (mean displacement) between corresponding landmarks per specimen in the sample when using the DTA to align the facial skeleton landmark set and the neurocranium landmark set under different conditions: green = using surface semilandmarks, yellow = triggering optional symmetrization procedure, red = using fixed landmark set only, and purple = using both surface semilandmarks and symmetry.

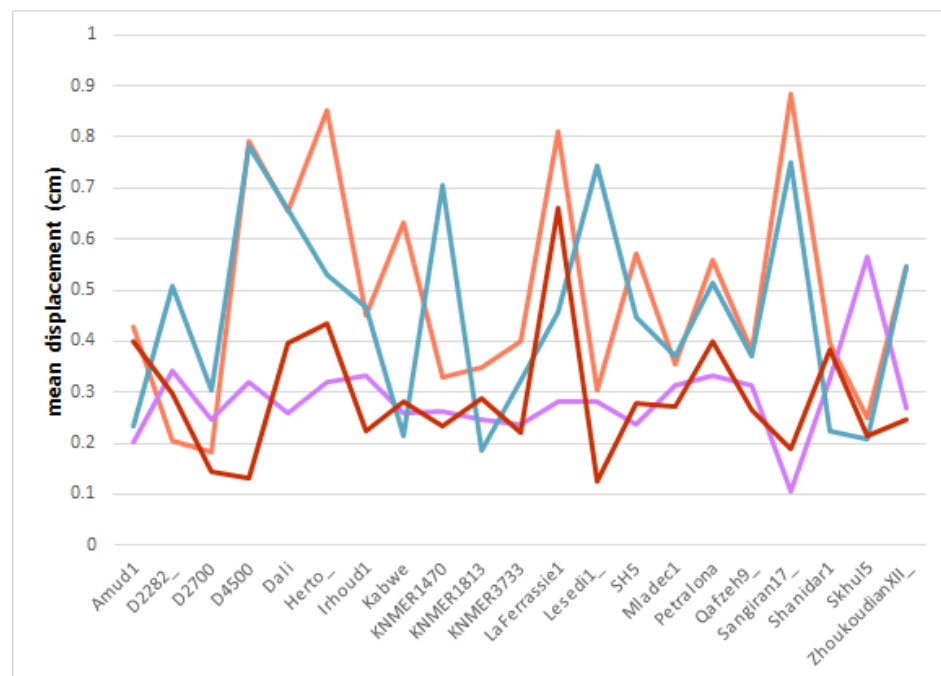


Figure 7. Mean Euclidean distance (mean displacement) between corresponding landmarks per specimen in the sample when using the DTA to align different fragment landmark sets under varying conditions: orange = alignment of facial skeleton with neurocranium using surface semilandmarks, teal = alignment of facial skeleton with neurocranium with fixed landmark set, purple = alignment of left supraorbital with neurocranium using surface semilandmarks, and red = alignment of left supraorbital with neurocranium using fixed landmarks.

Table 5. Two-factor analysis of variance (type II tests) of the Box-Cox transformed mean Euclidean distance estimated with and without using surface semilandmarks and the fragment of choice apart from the Ndutu neurocranium.

Effect	DFn	DFd	F Statistic	p Value	Ges
fragment choice	1	80	25.342	2.90×10^{-6} ^a	0.241000
semilandmarks	1	80	0.410	5.24×10^{-1}	0.005000
fragment choice:semilandmarks	1	80	0.067	7.96×10^{-1}	0.000838

^a Statistically significant.

Table 6. Estimated marginal means test of the Box-Cox transformed mean Euclidean distance estimated with and without using surface semilandmarks and the fragment of choice apart from the Ndutu neurocranium.

Fragment of Choice	Variable	y	Level 1	Level 2	df	Statistic	p Value ¹
Facial skeleton	semilandmarks	mean Euclidean distance	no	yes	80	−0.636	0.527 ²
Left supraorbital fragment	semilandmarks	mean Euclidean distance	no	yes	80	−0.270	0.788 ²

¹ Bonferroni adjusted. ² Not significant.

Based solely on descriptive statistics, the points located on the facial portion of the crania were estimated to be 0.492 cm from their original position on average. The best alignment of the facial landmarks of the sample appeared to have been achieved without using semilandmarks to sample the squamae's surface. The estimated position of the landmarks in the face was only 0.454 cm away from their original location on average. The results also varied less, with a standard deviation of 0.194 sd (compared with the 0.213 sd of the semilandmarks test). On the other hand, using sliding surface semilandmark information to estimate the location of the left supraorbital fragment apparently facilitated only slightly better and more consistent results, returning a mean = 0.288 cm and a standard deviation of 0.084.

To better understand the effect of applying surface semilandmarks, we performed a factorial ANOVA, as well as a series of post hoc tests, including the computation of estimated marginal means. However, the results of the preliminary application of the Shapiro–Wilk and Levene test revealed that in neither case did the data comply with the assumptions of normality or homoscedasticity. Hence, the data from both sets of tests were appropriately transformed.

The ANOVA on the Box-Cox normalized data (Table 5) yielded no statistically significant effect of the application of surface semilandmarks. Only the act of choosing a given fragment to align with the neurocranium affected the results ($F(1, 80) = 25.342$, $p = 0.00029$). A post hoc ungrouped pairwise *t* test confirmed the absence of a statistically significant difference whenever semilandmarks were being used to capture the squamous morphology ($p = 0.574$, Bonferroni adjusted). A grouped estimated marginal means test (Table 6) further confirmed this by establishing that there were no statistically significant differences between the results of applying surface semilandmarks and using an exclusively fixed landmark set for both the facial skeleton (statistic = -0.636 , $p = 0.527$, Bonferroni adjusted) and the left supraorbital (statistic = -0.27 , $p = 0.788$, Bonferroni adjusted).

The information gathered from these tests was used to inform the decisions taken to align the disarticulated fragments of the Ndutu cranium. Consequently, we chose to first execute the DTA to align the facial skeleton and neurocranium fragments, applying symmetry constraints and a data set comprised exclusively of fixed landmarks. In this instance, the DTA automatically selected SH 5 as the template, given the similitude between the landmark configurations of each fragment and the location of the same landmarks on that specimen. Subsequently, we decided to align the left supraorbital fragment with the facial skeleton and neurocranium composite model using only fixed landmarks and no additional provisions. Unsurprisingly, SH 5 was again selected by the tool as the template,

given the affinity resulting from the previous run of the DTA. Figure 8 illustrates the outcome of the digital alignment procedure.

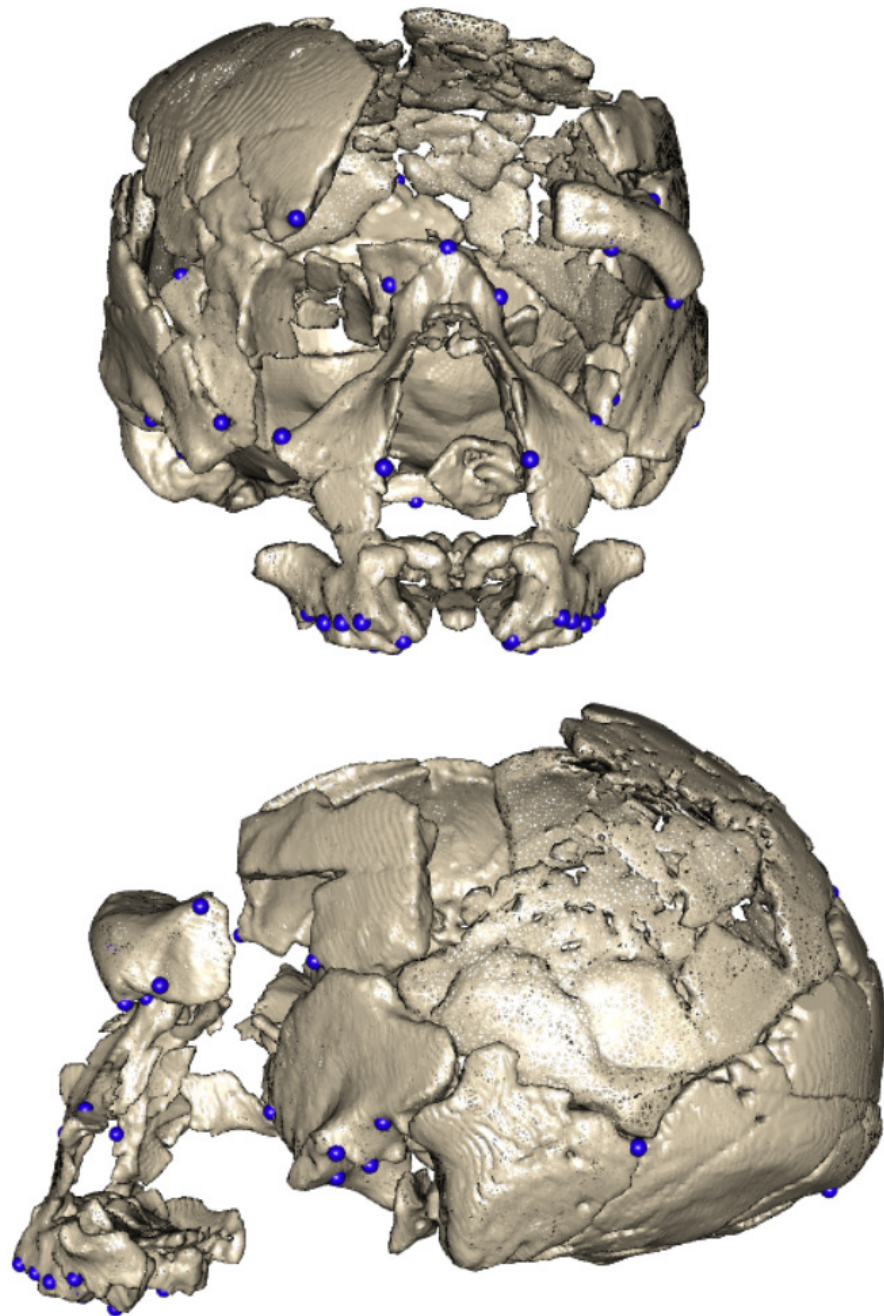


Figure 8. Aligned facial skeleton fragment cluster, left supraorbital fragment, and neurocranium fragment cluster. Frontal and lateral view.

As outlined in Section 2, the anatomy missing from the resulting AM was completed via TPS interpolation. Once this estimation of the parietal surface was obtained, we set to correct the plastic deformation on the anterior right parietal that, as noted in [4] and Clarke [3], provided it with an exaggeratedly bossed contour. To this aim, we retrodeformed a thick fragment in this region (see Figure 5). The final outcome of this and previous procedures was the new virtual reconstruction of the Ndotu cranium, which is presented in Figure 9.

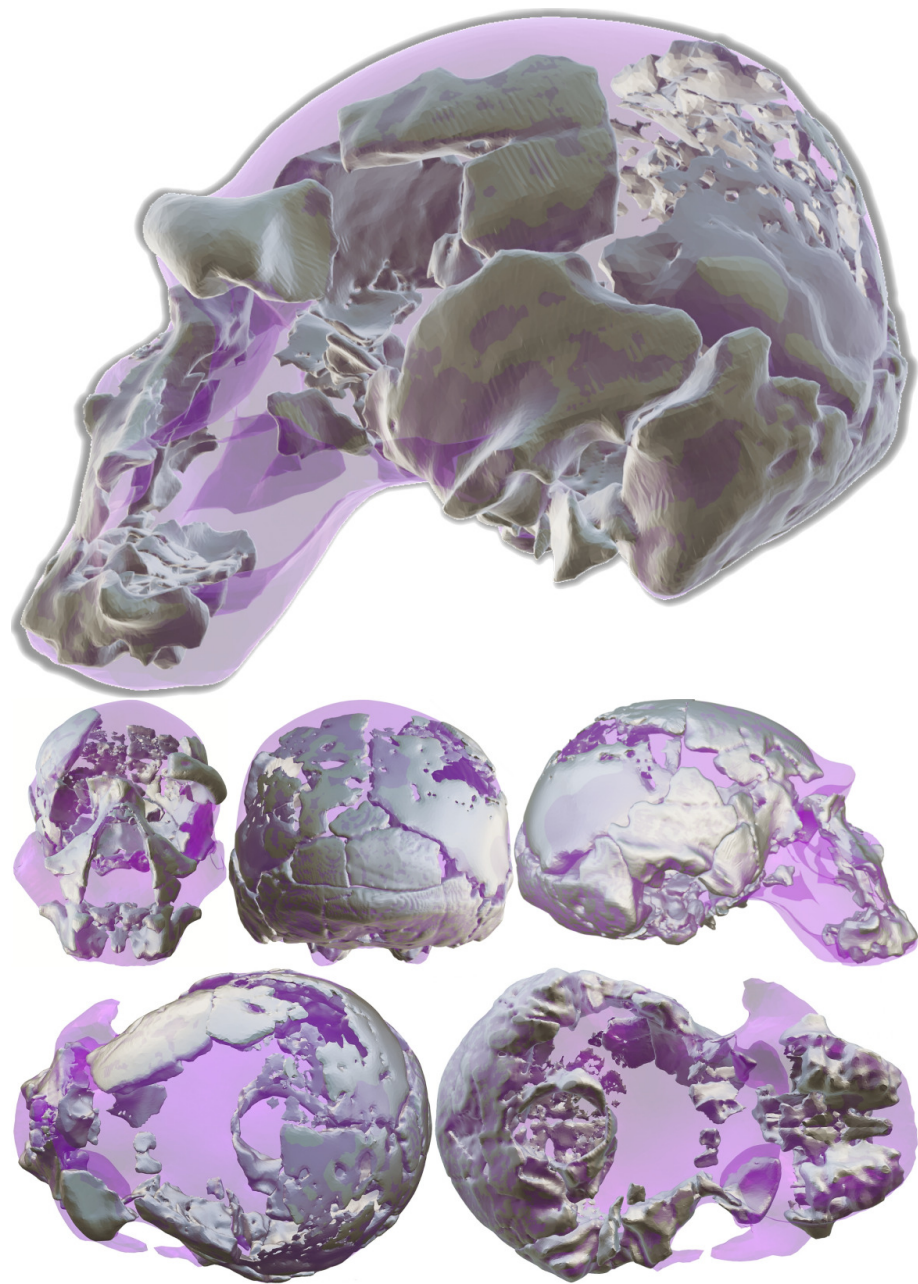


Figure 9. A new virtual reconstruction of the Ndutu cranium.

3.3. Geometric Morphometrics

As described in the previous section, the landmark configuration of our reconstruction was compared with that of Clarke's reconstruction via a GPA using a subset of the fixed landmark set based on the craniometric points observable in both models (Table 7). We subsequently created a deformation grid plotting the 1990 reconstruction to the one presented in this work (Figure 10). This allowed us to visualize how our reconstruction of Ndutu has a lower, more projected facial skeleton. Furthermore, the facial skeleton is projected in such an angle that it produces a more prognathic profile. Our reconstruction also possesses a narrower cranial vault than Clarke's. The left supraorbital fragment has also been estimated to be less protruding and closer to the midline.

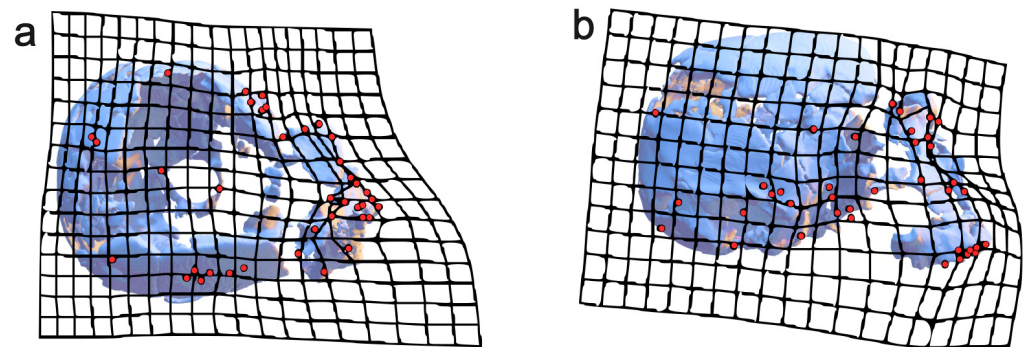


Figure 10. Composite of AM model and TPS deformation grids comparing the position of the landmarks on the articulated and disarticulated fragments of the Ndutu cranium in the model reassembled using CT-scan No. 1 (which boasts the the facial skeleton and supraorbital fragments as aligned by R. J. Clarke [3]) and the AM landmark set. The target shape is the AM, while the source is the reassembled model that includes Clarke’s alignment. The black dots correspond to a subset of the fixed landmark set (see Table 7). (a) X, Y TPS grid (superior view). (b) Y, Z TPS grid (lateral view).

Table 7. List of landmarks and semilandmarks employed in TPS deformation grid.

Landmarks
Left buccal M2
Left buccal M1
Left buccal P4
Left buccal P3
Left buccal C
Left lingual M1
Left lingual P4
Left lingual P3
Left lingual C
Left/right alare
Left/right zygoorbitale
Mid-torus inferior
Left/right maxillofrontale
Nasion
Left frontomolare orbitale
Left frontomolare temporale
Left/right frontotemporale
Left/right sphenion
Left/right superior infratemporal fossa
Left/right porion
Left/right asterion
Lambda
Inion
Left/right posterior glenoid point
Left/right lateral glenoid point
Left/right anterior glenoid point
Opisthion
Basion

The subsequent comparison of the sagittal profile of the specimens in the sample (Figure 11) using the landmark set in Table 8 confirmed that Ndutu’s reconstructed cranial outline is closest in shape (as indicated by the plot) to a small cluster of hominins, including not only Kabwe and La Ferrasie 1 but Suzuki and Takai’s [43] Amud 1 reconstruction as well. Although quite close to all of these, Ndutu is most similar in terms of cranial flexion, facial projection, supraorbital protrusion, and relative cranial height, length, and

nasion–prosthion length to Kabwe, overall. The La Ferrassie 1 cranium resulted the closest in terms of cranial flexion, facial projection, supraorbital protrusion, and even cranial height to our reconstruction of Ndotu, but not nearly as much as Kabwe or Suzuki and Takai’s Amud cranium when the rest of the traits in this study are taken into account.

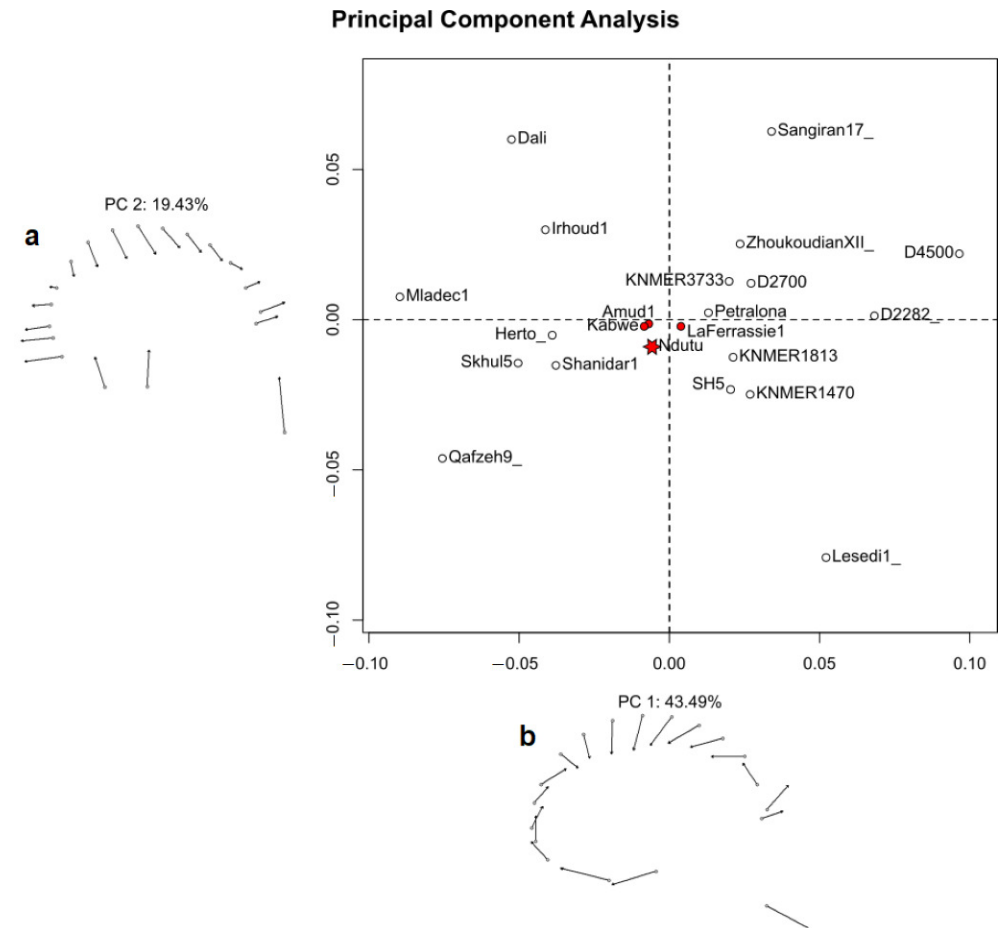


Figure 11. Shape variation across the sample using the sagittal profile landmark set. Principal component scores along PC1 and PC2 of the sagittal profiles of the specimens in the reference sample and the current reconstruction of the Ndotu cranium. The Ndotu cranium is represented by a red six-point star. Red circles depict the specimens closest in shape to Ndotu. (a) Vector plot illustrating shape variation along PC2. (b) Vector plot illustrating shape variation along PC1.

Table 8. List of landmarks and semilandmarks employed in the sagittal profile PCA.

Landmarks
Prosthion
Nasion
Glabella
8 midline curve semilandmarks on the cranial vault
Lambda
4 midline curve semilandmarks on occipital squama
Inion
Opisthion
Basion

Then, the interpolated squamous surface of Ndotu’s neurocranium, alongside the position of the fixed basicranial landmarks, were compared with the reference sample via a PCA. We illustrate the results of this shape analysis in Figure 12 and list the landmarks

employed in Table 9 (for the landmark definitions, please consult the Supplementary Information document Table S1).

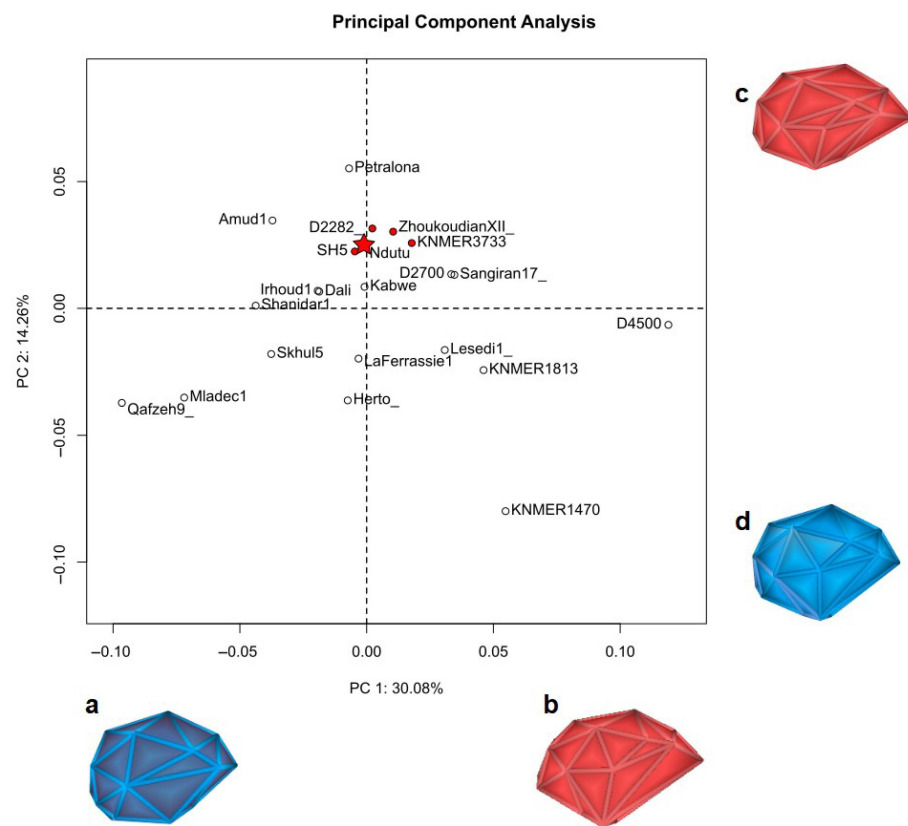


Figure 12. Shape variation across the sample using the neurocranium landmark set. Principal component scores along PC1 and PC2 of the outer surface of the frontal, temporal, parietal, occipital squamae, and left supraorbital of the specimens in the reference sample and the current reconstruction of the Ndutu cranium. The Ndutu cranium is represented by a red six-point star. Red circles depict the specimens closest in shape to Ndutu. (a) Shape of minimum value specimen neurocranium along PC1; (b) shape of maximum value specimen neurocranium along PC1; (c) shape of maximum value specimen neurocranium along PC2; and (d) shape of minimum value specimen neurocranium along PC2.

Table 9. List of landmarks and semilandmarks employed in the neurocranium PCA.

Landmarks
Left midtorus inferior
Left frontomale orbitale
Left frontomale temporale
Left/right frontotemporale
Left/right sphenion
Left/right superior infratemporal fossa
Left/right porion
Left/right asterion
Lambda
Inion
Left/right posterior glenoid point
Left/right lateral glenoid point
Left/right anterior glenoid point
Opisthion
Glabella
20 surface semilandmarks on the cranial vault

In this PCA, Ndutu is plotted (not unexpectedly) closest to cranium 5 of SH. The D2282 specimen from Georgia also resulted quite alike our reconstruction of Ndutu's neurocranium geometry. Semilandmarks located on the top, rear, and sides of the cranial vault describe a similar overall shape. This is supported by the relative position of both asterions and the degree of parietal bossing, which are alike in all three specimens.

Along PC1, the protrusion of the supraorbital torus as indicated by the reconstructed glabella, as well as the postorbital constriction manifested by the landmarks on the preserved left supraorbital fragment, strongly associates our reconstruction with the SH5 and D2282 individuals. Additionally, it is noteworthy that the Kabwe specimen returned a similar PC score along the first component.

On the other hand, changes along PC2 (accounting for 14.3% of the variation), mostly owing to the differences in the position of the fixed landmarks found on the basicranium, suggest a similitude with the Zhoukoudian XII and KNM ER 3733 exemplars. In our study, this component predominantly signals variance in terms of the posterior width of the cranial base.

4. Discussion

4.1. Digital Alignment

During the alignment phase of this reconstruction, we envisioned the use of two nonessential techniques to produce a well-informed, coherent reconstruction of the Ndutu cranium: the DTA's optional symmetrization procedure and the addition of surface semilandmarks to the fixed landmark set. Wary of the need to base our choice on evidence, we set out to first determine the convenience of using either approach. Thus, a series of tests and analyses were carried out, whose results are somewhat unexpected, particularly those concerning the alignment of the left supraorbital fragment.

On one hand, we speculated that the use of a symmetrical landmark set would allow to more accurately estimate the position of a mirrored version of the facial skeleton with Ndutu's relatively symmetrical neurocranial assemblage. Despite the use of the optional symmetrization procedure being associated with a lower average alignment error, no meaningful differences were observed between the results of the test performed with and without it. Therefore, we preliminarily attempted to align the mirrored facial skeleton with the neurocranium without symmetrization. Still, the resulting aligned model was moderately, yet visibly, askew.

Considering the fact that the specimens in the sample possessed differing levels of asymmetry, we resolved that the observed decrease in performance was due to Ndutu's particular degree of unevenness. Consequently, we aligned the facial skeletal fragment cluster while defining two sets of paired landmarks to trigger the DTA's symmetrization subprocess.

On the other hand, we conjectured that the use of semilandmarks should offer good results, because it would allow to sample points in the neurocranial squamae that would have otherwise been absent from the configuration and rendered our data unrepresentative of the entirety of the fossil's morphology. In the tests results presented in this work, however, the use of surface semilandmarks was associated with a considerably large estimation error.

Our current knowledge of the mechanisms underlying evolution warns that there could be additional forces at play. In this case, we posit that the likely culprits are the notions of integration and modularity [44]. Integration is defined as the interrelation and ontogenic codependency between traits or modules that are interconnected by genes, developmental mechanics, and spatial relationships [45]. Modules are highly integrated anatomical and functional units that are evolutionarily persistent (appear repeatedly in the fossil record) and respond independently to selective pressures [46]. In the literature on this subject, the human skull has been divided by many into several modules. Since 1982, Cheverud has distinguished two main modules: the neurocranial module and the orofacial module. However, he subdivided them into many more, including the frontal, parietal, and occipital subunits for the neurocranium and the frontal, orbital, nasal, oral, and masticatory subunits

for the orofacial. Other authors have recognized a variable number of other modules and assigned them different names (e.g., see Sardi et al. [47], González-José et al. [48]).

However, modules are not discrete units: although more correlated within themselves than with other modules, they have been shown to influence the evolutionary trajectory of neighboring structures [49]. For example, it has been postulated that, in the evolution of the genus *Homo*, the size of the brain and the consequent expansion of the basicranium are coupled with a greater degree of cranial flexion. Likewise, as the facial size increases, so does the distance between the temporomandibular joint and the dental arch, that is, cranial flexion decreases [45].

Thus, what this implies is that one possible explanation of why sampling the cranial vault yielded poor results when estimating the position of the facial skeleton is that surfaces whose morphology was recorded with semilandmarks belong to a distinct module. In fact, landmarks that describe the characteristics of the temporomandibular joint, and those that describe the expansion of the cranial base that could be better predictors of these spatial relationships, are proportionally better represented in the set of fixed landmarks.

A similar logic could be employed to interpret the unforeseen results concerning the use of surface semilandmarks to estimate the position of the left supraorbital fragment. When this sampling technique is used on a discontinuous surface, semilandmarks are bound to be unevenly distributed among the fragments covering more and less surface area. Because the preserved frontal squamous surface is smaller than that of the preserved temporal, parietal, and occipital squamae, only a few semilandmarks are placed on it. Thus, fewer data from this adjacent module can be used to align the supraorbital fragment.

4.2. Shape Affinities

In view of the test results, we settled on aligning the Ndotu fragments following a mixed approach where symmetry was only taken into consideration while estimating the position of the facial skeleton, whereas the supraorbital fragment was subsequently aligned using only fixed landmarks while disregarding symmetry. Upon execution, the DTA algorithm selected the SH 5 cranium as the best template to reconstruct the Ndotu cranium both in the first and second round.

Evidently, the DTA's choice of SH 5 as the template in the first run of the script influenced subsequent executions and other reconstruction efforts. However, the DTA's assessment resonates with the findings of Arsuaga et al. [6]. Bearing in mind the fact that the landmarks included in the fixed set used in this work include most of the craniometric points in that study, and considering the absence of Steinheim and Tabun 1 from the sample, we deem the DTA's assignment of SH 5 as the template unsurprising. Like SH5, and as noted by Clarke in [3], Ndotu displays a rather round occipital. Furthermore, it shares with the SH crania and with those attributed to *H. erectus* the presence of an occipital torus—albeit a somewhat faint one.

Clarke argued that Ndotu displayed a trait complex exclusive to the *sapiens* lineage, which included, aside this occipital “roundness”, a notable amount of parietal bossing. Nonetheless, in neither instance did our reconstruction, now lacking the exaggerated bossing of the right parietal, show any affinities with specimens attributed to the *sapiens* lineage, such as Irhoud 1, Herto, Skhul V or Qafzeh 9. Instead, the PCA that was executed using data from the interpolated parietal surface of the Ndotu cranium also conceded a propinquity with SH 5 as expected.

Perhaps least foreseen were the results of our sagittal profile study which, despite not lending support to Clarke's observations either, suggested a similitude with different group of hominins, most notable among which was the Kabwe cranium. As commented in the introduction of this work, Rightmire [9] judged that the Ndotu cranium height, length, and flexion, alongside its facial height and projection, may have been closest to the range of a group of robust, Late Pleistocene hominins, which included Kabwe. Furthermore, the results of the subsequent comparison between the reconstructed neurocranial morphology of Ndotu and the reference sample granted a few more traits associating Ndotu with

Kabwe, such as substantial postorbital constriction and a wide neurocranium—both of which are featured among Rightmire’s criteria for membership in the same paleo-deme as that specimen.

This outcome may be interpreted as suggestive of some agreement with the notion that the inclusion of Ndutu was justified. Yet, regardless of how tempting that may be, it must be taken in to account that Kabwe’s own membership to such a group has been challenged by Grün [8].

Exemplars such as Bodo, Saldanha or Zuttiyeh may offer a way to further cement Ndutu’s belonging to this group, but they are absent from our reference sample since their preservation frustrated their inclusion. Additionally, other traits whose nature could be described morphometrically via an alternative set of landmarks or, most certainly, morphoscopically via the detailed assessment of their anatomy, still bear the potential to paint a clearer picture of Ndutu’s phylogenetic affinities. Therefore, the results dispensed here are still preliminary. The phylogeny of Ndutu is a complex matter that should be settled by means of a comprehensive consideration of its preserved anatomy, for which this work is intended to serve as a fundament.

As Lautenschlager [11] impeccably warns, the products of digital reconstruction efforts should be regarded as amendable hypotheses. Thus, it is imperative to admit that the current state of the Ndutu reconstruction is susceptible to improvement upon the advancement of the techniques and materials available, and collaborator contributions. Regardless, if the reconstruction hypothesis presented in this work is held, Ndutu’s inclusion in future morphological studies is granted.

5. Conclusions

The Ndutu cranium is a valuable fragmentary fossil specimen excavated from Upper Acheulean strata dated c. 450 Ka BP [2] at the Lake Ndutu site, Tanzania [1]. Prior to its recovery, it was subject to taphonomic distortion [3]. Hence, it was reconstructed manually in 1976 by Clarke and then again in 1978 after the addition of newly found fragments (this last reconstruction was published in 1990).

The morphology of the fossil has been studied and its phylogenetic affinities discussed by various authors [3,4,6,7,9,13,14]. Despite this, there is no consensus on the status of the Ndutu cranium. This is partly owed to the fact that, up until now, Ndutu had remained a specimen reconstructed following a now outdated approach that has been since criticized for its exaggeration of *sapiens* features [4].

In this paper, we present new virtual reconstruction of the Ndutu cranium. We detail the preparation of the 3D models, the reassembly the articulated fragments, the mirroring of the facial skeleton, the digital alignment of the disarticulated fragments, the completion of the cranium’s missing features, and the retrodeformation of a single fragment in the anterior right parietal. We also report on the results of a small series of tests undertaken with the aim of informing our decisions regarding the digital alignment. Finally, we perform a morphological comparison of our reconstruction by means of a GM approach.

This new virtual reconstruction of Ndutu possesses a lower, more prognathic facial profile, along with a narrower cranial vault and a less projected and narrower supraorbital torus. Devoid of its exaggerated parietal bosses, our rendering of the Ndutu cranial vault resulted anticipatedly close in overall shape to the specimen that was selected as a template during reconstruction: SH 5. Less expectedly, however, the reconstructed geometry of the sagittal profile of Ndutu turned out similar to that of Kabwe. Although only further work shall settle the argument regarding Ndutu’s phylogeny, our transparent approach has granted its inclusion in future morphological studies.

Supplementary Materials: The following supporting information can be downloaded at: <https://www.mdpi.com/article/10.3390/heritage6030151/s1>, Table S1: Number, code, name, and definition of the landmarks in this study; Table S2: Descriptive statistics of surface semilandmarks test results; Table S3: Shapiro–Wilk test of normality on model residuals of surface semilandmarks test results; Table S4: Shapiro–Wilk test of normality on surface semilandmarks test results; Table S5: Levene

test for the equality of variances on surface semilandmarks test results; Table S6: Shapiro–Wilk test of normality on model residuals of transformed data of surface semilandmarks test results; Table S7: Shapiro–Wilk test of normality on transformed data of surface semilandmarks test results; Table S8: Levene test for the equality of variances on transformed data of surface semilandmarks test results; Table S9: Descriptive statistics of surface semilandmarks versus symmetrization test results; Table S10: Shapiro–Wilk test of normality on model residuals of surface semilandmarks versus symmetrization test results; Table S11: Shapiro–Wilk test of normality on surface semilandmarks versus symmetrization test results; Table S12: Levene test for the equality of variances on surface semilandmarks versus symmetrization test results. R scripts written for this work are publicly available at: <https://github.com/gustavodmh/ndutu-dta> (accessed on 27 December 2022).

Author Contributions: Conceptualization, C.L. and G.M.; methodology, G.M.; software, C.L. and G.M.; validation, G.M.; formal analysis, G.M.; investigation, G.M.; resources, C.L.; data curation, C.L.; writing—original draft preparation, G.M.; writing—review and editing, C.L.; visualization, G.M.; supervision, C.L.; project administration, C.L. All authors have read and agreed to the published version of the manuscript.

Funding: The first author (G.M.) received an Erasmus Mundus scholarship funded by the EACEA, European Commission. The second author (C.L.) received the ICREA Academia 2022 distinction and takes part in the following funded projects: Period 2022–2026 Social, cultural, and biological Evolution during the Pleistocene (StEP). Generalitat de Catalunya, AGAUR SGR2021. IP: Andreu Ollé.; Period 2022–2025 Geology, geochronology and Paleobiology of the Sierra de Atapuerca sites VIII. MICIU No. PID2021-122355NB-C31. IP: Juan Luis Arsuaga & José Miguel Carretero.

Data Availability Statement: The 3D model of the new virtual reconstruction of the Ndutu cranium is available upon request to the authors.

Acknowledgments: The authors would like to express their gratitude to the following researchers: Antoine Balzeau and Florent Détroit, from the Muséum National d’Histoire Naturelle (Paris, France), and Jordi Agustí, researcher at IPHES-CERCA (Tarragona, Spain) for giving access to human fossils or replicas under their care. We would also like to thank all of the referees summoned by the MDPI editorial office for their keen observations and for the time and effort that they diligently put into reviewing our paper. Moreover, we would like to thank the University of Vienna, the University of the Witwatersrand, Duke University, the Peabody Museum, and the African Fossils team for sharing their superb 3D materials via their respective repositories. Finally, the first author (G. M.) would like to thank the Erasmus Mundus program of the European Commission and the International Master in Quaternary and Prehistory (IMQP) consortium for providing the necessary funding, opportunities, and support for the development of the master’s thesis from which this work originates, despite the global pandemic.

Conflicts of Interest: The authors declare no conflict of interest.

Abbreviations

The following abbreviations are used in this manuscript:

IPHES-CERCA	Institut Català de Paleoeologia Humana i Evolució Social
FOV	Field of view
H.	<i>Homo</i>
SH	Sima de los Huesos (site)
DTA	Digital Alignment Tool
ANOVA	Analysis of Variance
GPA	General Procrustes Analysis
PCA	Principal Component Analysis
TPS	Thin-plate spline

References

1. Mturi, A. New hominid from Lake Ndutu, Tanzania. *Nature* **1976**, *262*, 484–485. [[CrossRef](#)]
2. Manega, P.C. Geochronology, Geochemistry and Isotopic Study of the Plio-Pleistocene Hominid Sites and the Ngorongoro Volcanic Highland in Northern Tanzania. Ph.D. Thesis, University of Colorado at Boulder, Boulder, CO, USA, 1993.
3. Clarke, R.J. The Ndutu cranium and the origin of *Homo sapiens*. *J. Hum. Evol.* **1990**, *19*, 699–736. [[CrossRef](#)]
4. Rightmire, G.P. The Lake Ndutu cranium and early *Homo sapiens* in Africa. *Am. J. Phys. Anthropol.* **1983**, *61*, 245–254. [[CrossRef](#)]

5. Hublin, J.J. Northwestern African Middle Pleistocene hominids and their bearing on the emergence of Homo sapiens. In *Human Roots, Africa and Asia in the Middle Pleistocene*; Western Academic and Specialist Press: Barnsley, UK, 2002; pp. 99–121.
6. Arsuaga, J.L.; Martínez, I.; Gracia, A.; Lorenzo, C. The Sima de los Huesos crania (Sierra de Atapuerca, Spain): A comparative study. *J. Hum. Evol.* **1997**, *33*, 219–281. [[CrossRef](#)]
7. Stringer, C. The origin and evolution of Homo sapiens. *Philos. Trans. R. Soc. B Biol. Sci.* **2016**, *371*, 20150237. [[CrossRef](#)] [[PubMed](#)]
8. Grün, R.; Pike, A.; McDermott, F.; Eggins, S.; Mortimer, G.; Aubert, M.; Kinsley, L.; Joannes-Boyau, R.; Rumsey, M.; Denys, C.; et al. Dating the skull from Broken Hill, Zambia, and its position in human evolution. *Nature* **2020**, *580*, 372–375. [[CrossRef](#)] [[PubMed](#)]
9. Rightmire, G.P. Middle Pleistocene Homo Crania from Broken Hill and Petralona: Morphology, metric comparisons, and evolutionary relationships. In *Human Paleontology and Prehistory*; Springer: Berlin/Heidelberg, Germany, 2017; pp. 145–159.
10. Roksandic, M.; Radović, P.; Wu, X.; Bae, C.J. Resolving the “muddle in the middle”: The case for Homo bodoensis sp. nov. *Evol. Anthropol. Issues News Rev.* **2022**, *31*, 20–29. [[CrossRef](#)]
11. Lautenschlager, S. Reconstructing the past: Methods and techniques for the digital restoration of fossils. *R. Soc. Open Sci.* **2016**, *3*, 160342. [[CrossRef](#)]
12. Eslami, D.; Di Angelo, L.; Di Stefano, P.; Pane, C. Review of computer-based methods for archaeological ceramic sherds reconstruction. *Virtual Archaeol. Rev.* **2020**, *11*, 34. [[CrossRef](#)]
13. Schwartz, J.H.; Tattersall, I. *The Human Fossil Record, Craniodental Morphology of Genus Homo (Africa and Asia)*; John Wiley & Sons: Hoboken, NJ, USA, 2005; Volume 2.
14. Clarke, R.J. New cranium of Homo erectus from Lake Ndutu, Tanzania. *Nature* **1976**, *262*, 485–487. [[CrossRef](#)]
15. Weber, G.W.; Seidler, H.; Magori, C.; Saanane, C.; Kamamba, D.; Thackeray, F.; Schrenk, F.; Recheis, W.; Nedden, D.Z.; Conroy, G.C. *NDUTU, CD-ROM Including Data from CT-Scans*; Department of Evolutionary Anthropology, University of Vienna: Vienna, Austria; Department of Antiquities, Dar-es-Salaam: Dar es Salaam, Tanzania, 2005.
16. Materialise NV. *Mimics Medical (Software)*; Materialise NV: Leuven, Belgium, 2017.
17. Cignoni, P.; Callieri, M.; Corsini, M.; Dellepiane, M.; Ganovelli, F.; Ranzuglia, G. MeshLab: An Open-Source Mesh Processing Tool. In Proceedings of the Eurographics Italian Chapter Conference, Salerno, Italy, 2–4 July 2008; Scarano, V., Chiara, R.D., Erra, U., Eds.; The Eurographics Association: Vienna, Austria, 2008. [[CrossRef](#)]
18. Agisoft LLC. *AgiSoft PhotoScan Standard (Version 1.4.0) (Software)*; Agisoft LLC: St. Petersburg, Russia, 2017.
19. Papaioannou, G.; Schreck, T.; Andreadis, A.; Mavridis, P.; Gregor, R.; Sipiran, I.; Vardis, K. From Reassembly to Object Completion. *J. Comput. Cult. Herit.* **2017**, *10*, 1–22. [[CrossRef](#)]
20. Palmas, G.; Pietroni, N.; Cignoni, P.; Scopigno, R. A computer-assisted constraint-based system for assembling fragmented objects. In *Digital Heritage International Congress*; The Eurographics Association: Vienna, Austria, 2013. [[CrossRef](#)]
21. Profico, A.; Buzi, C.; Davis, C.; Melchionna, M.; Veneziano, A.; Raia, P.; Manzi, G. A New Tool for Digital Alignment in Virtual Anthropology. *Anat. Rec.* **2019**, *302*, 1104–1115. [[CrossRef](#)]
22. Gower, J.C. Generalized procrustes analysis. *Psychometrika* **1975**, *40*, 33–51. [[CrossRef](#)]
23. Rohlf, F.J.; Slice, D. Extensions of the Procrustes Method for the Optimal Superimposition of Landmarks. *Syst. Zool.* **1990**, *39*, 40. [[CrossRef](#)]
24. White, T.D.; Black, M.T.; Folkens, P.A. *Human Osteology*; Academic Press: Cambridge, MA, USA, 2012.
25. Stelzer, S.; Neubauer, S.; Hublin, J.J.; Spoor, F.; Gunz, P. Morphological trends in arcade shape and size in Middle Pleistocene Homo. *Am. J. Phys. Anthropol.* **2019**, *168*, 70–91. [[CrossRef](#)]
26. McNulty, K.P. A geometric morphometric assessment of the hominoid supraorbital region: Affinities of the Eurasian Miocene hominoids Dryopithecus, Graecopithecus, and Sivapithecus. In *Modern Morphometrics in Physical Anthropology*; Springer: Berlin/Heidelberg, Germany, 2005; pp. 349–373.
27. Martin, R.; Saller, K. *Lehrbuch der Anthropologie III*; Gustav Fischer: Stuttgart, Germany, 1957.
28. Smith, H.F.; Ritzman, T.; Otárola-Castillo, E.; Terhune, C.E. A 3-D geometric morphometric study of intraspecific variation in the ontogeny of the temporal bone in modern Homo sapiens. *J. Hum. Evol.* **2013**, *65*, 479–489. [[CrossRef](#)] [[PubMed](#)]
29. Bookstein, F.L. *Morphometric Tools for Landmark Data: Contents*; Cambridge University Press: Cambridge, UK, 1992; pp. v–xii.
30. Bookstein, F.L. *Morphometric Tools for Landmark Data: Geometry and Biology*; Cambridge University Press: Cambridge, UK, 1997.
31. Gunz, P.; Mitteroecker, P.; Bookstein, F.L. Semilandmarks in Three Dimensions. In *Modern Morphometrics in Physical Anthropology*; Slice, D.E., Ed.; Springer: Boston, MA, USA, 2005; pp. 73–98. [[CrossRef](#)]
32. Gunz, P.; Mitteroecker, P. Semilandmarks: A method for quantifying curves and surfaces. *Hystrix Ital. J. Mammal.* **2013**, *24*, 103–109.
33. Bardua, C.; Felice, R.N.; Watanabe, A.; Fabre, A.C.; Goswami, A. A Practical Guide to Sliding and Surface Semilandmarks in Morphometric Analyses. *Integr. Org. Biol.* **2019**, *1*, obz016. [[CrossRef](#)] [[PubMed](#)]
34. Roth, V. On three-dimensional morphometrics, and on the identification of landmark points. In *Contributions to Morphometrics*; Museo Nacional de Ciencias Naturales: Madrid, Spain, 1993; Volume 41, p. 61.
35. Zelditch, M.; Swiderski, D.; Sheets, H.D.; Fink, W. *Geometric Morphometrics for Biologists: A Primer*; Academic Press: Cambridge, MA, USA, 2004. [[CrossRef](#)]
36. Madrigal, L. *Statistics for Anthropology*; Cambridge University Press: Cambridge, UK, 2012.
37. Peterson, R.A. Finding Optimal Normalizing Transformations via bestNormalize. *R J.* **2021**, *13*, 310–329. [[CrossRef](#)]

38. Adams, D.; Collyer, M.; Kaliontzopoulou, A.; Baken, E. Geomorph: Software for Geometric Morphometric Analyses. R package version 4.0., 2021. <https://cran.r-project.org/package=geomrph> (accessed on 27 December 2022).
39. Community, B.O. *Blender—A 3D Modelling and Rendering Package*; Blender Foundation, Stichting Blender Foundation: Amsterdam, The Netherlands, 2018.
40. 3D Slicer Image Computing Platform; BWH and 3D Slicer Contributors, 16 November 2022. <https://www.slicer.org/> (accessed on 27 December 2022).
41. Fedorov, A.; Beichel, R.; Kalpathy-Cramer, J.; Finet, J.; Fillion-Robin, J.C.; Pujol, S.; Bauer, C.; Jennings, D.; Fennessy, F.; Sonka, M.; et al. 3D Slicer as an image computing platform for the Quantitative Imaging Network. *Magn. Reson. Imaging* **2012**, *30*, 1323–1341. [[CrossRef](#)]
42. Mitteroecker, P.; Huttegger, S.M. The concept of morphospaces in evolutionary and developmental biology: Mathematics and metaphors. *Biol. Theory* **2009**, *4*, 54–67. [[CrossRef](#)]
43. Suzuki, H.; Takai, F. *The Amud Man and His Cave Site*; Academic Press of Japan: Tokyo, Japan, 1970.
44. Gunz, P.; Mitteroecker, P.; Neubauer, S.; Weber, G.W.; Bookstein, F.L. Principles for the virtual reconstruction of hominin crania. *J. Hum. Evol.* **2009**, *57*, 48–62. [[CrossRef](#)]
45. Lieberman, D.E. 16. Epigenetic Integration, Complexity, and Evolvability of the Head: Rethinking the Functional Matrix Hypothesis. In *Epigenetics*; University of California Press: Berkeley, CA, USA, 2011; pp. 271–289.
46. Müller, G.B. Evo–devo: Extending the evolutionary synthesis. *Nat. Rev. Genet.* **2007**, *8*, 943–949. [[CrossRef](#)] [[PubMed](#)]
47. Sardi, M.L.; Ventrice, F.; Ramírez Rozzi, F. Allometries Throughout the Late Prenatal and Early Postnatal Human Craniofacial Ontogeny. *Anat. Rec.* **2007**, *290*, 1112–1120. [[CrossRef](#)] [[PubMed](#)]
48. González-José, R.; Escapa, I.; Neves, W.A.; Cúneo, R.; Pucciarelli, H.M. Cladistic analysis of continuous modularized traits provides phylogenetic signals in Homo evolution. *Nature* **2008**, *453*, 775–778. [[CrossRef](#)] [[PubMed](#)]
49. Cheverud, J.M. Phenotypic, genetic, and environmental morphological integration in the cranium. *Evolution* **1982**, *36*, 499–516. [[CrossRef](#)]

Disclaimer/Publisher’s Note: The statements, opinions and data contained in all publications are solely those of the individual author(s) and contributor(s) and not of MDPI and/or the editor(s). MDPI and/or the editor(s) disclaim responsibility for any injury to people or property resulting from any ideas, methods, instructions or products referred to in the content.